Heliyon 9 (2023) e19893

Contents lists available at ScienceDirect

Heliyon

journal homepage: www.cell.com/heliyon

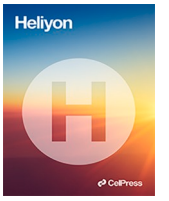

Cobalt ferrite nanoparticle for the elimination of CD133+CD44^{+} and CD44^{+}CD24^{-}, in breast and skin cancer stem cells, using non-ionizing treatments

Bahareh Khalili Najafabad [a,b], Neda Attaran [c], Mehdi Barati [d], Zahra Mohammadi [e], Mahmoud Mahmoudi [f,**], Ameneh Sazgarnia [a,b,*]

[a] Medical Physics Research Center, Mashhad University of Medical Sciences, Mashhad, Iran
[b] Department of Medical Physics, Faculty of Medicine, Mashhad University of Medical Sciences, Mashhad, Iran
[c] Department of Medical Nanotechnology, Applied Biophotonics Research Center, Science and Research Branch, Islamic Azad University, Tehran, Iran
[d] Department of Pathobiology and Laboratory Sciences, North Khorasan, University of Medical Science, Bojnurd, Iran
[e] Radiological Technology Department of Actually Paramedical Sciences, Babol University of Medical Science, Babol, Iran
[f] Immunology Research Center, Bu-Ali Research Institute, Faculty of Medicine, Mashhad University of Medical Sciences, Mashhad, Iran

ARTICLE INFO

Keywords:
Photothermal therapy (PTT)
Photodynamic therapy (PDT) and magnetic hyperthermia (MHT)
Cancer stem cell (CSC)
Superparamagnetic nanoparticle

ABSTRACT

Background: Cancer stem cells (CSCs) are the most challenging issue in cancer treatment, because of their high resistance mechanisms, that can cause tumor recurrence after common cancer treatments such as drug and radiation based therapies, and the insufficient efficiency of common treatments in CSCs removal and the recurrence of tumors after these treatments, it is essential to consider other methods, including non-ionizing treatments likes light-based treatments and magnetic hyperthermia (MHT).

Method and material: After synthesis, characterization and investigation, the toxicity of novel on A375 and MAD-MB-231 cell lines, magnetic hyperthermia and light-based treatments were applied. MTT assay and flow cytometry was employed to determine cell survival. the influence of combination therapy on CD44 + CD24^{-}and CD133 + CD44^{+} cell population, Comparison and evaluation of combination treatments was done respectively using Combination Indices (CIs).

Result: The final nanoparticle has a high efficiency in producing hydroxyl radicals and generating heat in MHT. According to CIs, we can conclude that combined using of light-based treatment and MHT in the presence of final synthesized nanoparticle have synergistic effect and a high ability to reduce the population of stem cells in both cell lines compared to single treatments.

Conclusion: In this study a novel multi-functional nanoplatform acted well in dual and triple combined treatments, and showed a good performance in the eradication of CSCs, in A375 and MAD-MB-231 cell lines.

* Corresponding author. Medical Physics Research Center, Mashhad University of Medical Sciences, Mashhad, Iran.
** Corresponding author. Immunology Research Center, Mashhad University of Medical Sciences, Mashhad, Iran.
E-mail addresses: Mahmoudim@mums.ac.ir (M. Mahmoudi), sazgarniaa@mums.ac.ir (A. Sazgarnia).

https://doi.org/10.1016/j.heliyon.2023.e19893
Received 3 June 2023; Received in revised form 2 September 2023; Accepted 5 September 2023
Available online 15 September 2023

1. Introduction

Nowadays magnetic nanoparticles (MNPs), owing to their unique features has been considered in various fields like biotechnology, biomedical (in some studies as a probe for detection), materials science, and engineering [1,2]. They can serve as carrier for drugs, contrast agent in MRI, and they can be used in hyperthermia as therapeutic agent which can induce heat [3]. Their high surface-to-volume ratio of these particles causes nanoparticle can load a lot of chemotherapy and sensitizing drugs, or delivering MNPs to the desired area by functionalizing them with special markers, for preventing side damage to other tissues [4]. In biological application superparamagnetic manners of magnetic nanoparticle is more important than ferromagnetism, tissues should have high magnetic susceptibility means that, which can quickly acquire magnetic properties and loses it by applying a magnetic field.

When it is cut off [5,6]. In biological applications it is important to use stable nanoparticle without aggregation. Several factors affect the stability of nanostructures like superficial electrical load, surface chemistry, and particle size; smaller nanoparticles show a smaller interparticle gravitational force [7]. Coating magnetic nanoparticle with a biodegradable material, like polyethylene glycol (PEG), can prevent their aggregation and keep the nanoparticle structure from changing off the initial state. In addition to the biodegradability benefits of these coatings, they can increase the drug loading or rise the chance of forming a covalent bond between the drug and the nanoparticle, what can increase drug's uptake and trapping [8], The type of coating, and the nature of MNP score as well as their size, which affects their biocompatibility. For example, the cytotoxicity of iron is lower than the other ferromagnetic materials. For this reason, in more studies, this element or its alloys are used [9]. In this study we use PEG and citric acid to increase both biocompatibility and stability. Magnetic nanoparticle can be targeted to the region of interest via magnetic field [10]. Moreover, that synthesis method can determine the amount of impurities and the dispersion of these impurities, hence it affects the behavior and magnetic attributes of the particles [11].

Magnetic hyperthermia is an auxiliary method of treatment which is used in combination of the other methods like chemotherapy and radiotherapy. In magnetic hyperthermia, an increase in temperature is the result of changes in the magnetic field in presence of MNPs [12]. It is classified as non-ionizing and non-destructive treatments [13,14]. Kharat et al. used PEG-coated $MnFe_2O_4$in their MHT cancer applications studies for its high heating potential [15]. In magnetic hyperthermia, the behaviors that induces this increase in temperature are Brownian Relaxation and Néel Relaxation of the MNPs inside the magnetic field (MF). Rising temperature can cause apoptosis, necrosis or thermal ablation [16]. The Fenton reaction is one of the reactions that occur in iron-based nanoparticles. In this reaction, endogenous hydrogen peroxide is changed to hydroxyl radicals which can stop the growth of the tumor. In addition, magnetic hyperthermia increases tumor acidity and also causes hypoxia [17]. Although it is used as adjuvant treatment beside conventional therapies like chemotherapy and radiotherapy, few studies have been accomplished on the effect of MHT on CSCs [18]. CSCs are subpopulation of tumor cells that have capability of self-renewing, repairing and can proliferate fast or being in quiescent phase [19]. They are resident to radiation and chemotherapy [20]. They have some special markers make them distinguishable. Some of these markers are well-known CSCs markers like CD24, CD44, CD166, CD133, EpCAM [21]. Their numbers are different in different tumors and this is the reason why some tumors are more aggressive than others [22]. In addition to magnetic hyperthermia. Studies have shown that light-based treatments had a great effect in eradicating stem cells. Considering the lack of research in the field of non-ionizing treatments against cancer cells, in addition to magnetic hyperthermia, photodynamic and photothermal methods were also used in this study.

Photodynamic therapy (PDT), and Photothermal therapy (PTT (are non-ionization methods that use light sensitizers and light with a wavelength proportionate with those sensitizers to treat cancer [23]. Both methods have few side effects and affect cancer cells more than healthy cells [24]. In photothermal therapy light is converted to heat by photosensitizers and cause ablation in tumors, but in photodynamic cell death mechanism is different and it is duo to (Reactive Oxygen Species) ROS production in exposed photosensitizers [25]. Several materials can be served as PTT and PDT agents like (Protoporphyrin IX) PpIX and (Indocyanine Green) ICG, respectively. They are utilized in various medical application for both therapy and diagnostic [26]. One of the advantages of using ICG as a photosensitizer is being (Food and Drug Administration FDA) approved in clinical users, stimulation in the near infrared region (NIR) around 800 nm with negligible fluorescence intrusion by biomolecules at this wavelength, and high production efficiency of the ROS [27]. However, its rapid excretion from the blood causes to use nanoparticles to encapsulate and load it in diagnostic and therapeutic applications to provide the necessary time for imaging and treatment [28]. Due to the negative charge of the ICG, this dye is electrostatically attached to the nanoparticles [29]. The ROS produced by photosensitizers with a very short half-life has a low diffusion rate, so after production only the adjacent cells can have a necrotic effect and other tissues are preserved. Therefore, considering the short lifespan of the ROS, sensitizer targeting to interested tissue is important [30]. Also, this agent has high photothermal efficiency, but it had to be used in nanosystem format in order to prevent plasma protein binding and degeneration, prolong biological half-life, be resistant to heat and light, so these features are the reason for our choice [31]. Due to the persistence of CSCs to common treatments such as drug-based and radiation-based treatments and the possibility of the survival of these cells after a common treatment and the recurrence of the tumor, it is necessary to suggest other treatments, including non-ionizing treatment. In addition, due to the fact that in our previous study, the effectiveness of treatments such as photodynamic and photothermal was proven in the annihilation of stem cells. In this study, the effect of MHT and its effectiveness as a pre-treatment along with the mentioned treatment were evaluated. There are many methods for the synthesis of MNPs, among which the co-precipitation method is better because it can produce particles with uniform size and structure. The more homogeneous particle is the best for MHT applications [32]. In this study we synthesized MNPs which were covered with citric acid and PEG to increase its biocompatibility and stability then conjugated with ICG as photothermal sensitizer and PpIX as photodynamic sensitizer, in order to perform treatment. The treatments efficiency was evaluated by flow cytometry test using human monoclonal antibodies like CD44, CD24, and CD133 as CSC markers.

2. Material and methods

2.1. Chemical materials

Protoporphyrin IX (PpIX) and Indocyanine green (ICG) from Merck company, Iron (III) sulfate, Cobalt (II) chloride from Aldrich were purchased. Other materials like RPMI 1640, DMEM, MTT, trypsin–EDTA and other material related to cell culture were bought from Sigma-Aldrich. Three monoclonal human anti body such as FITC anti-human CD24, PERCP/Cyanine5.5 anti-human CD44 and PE

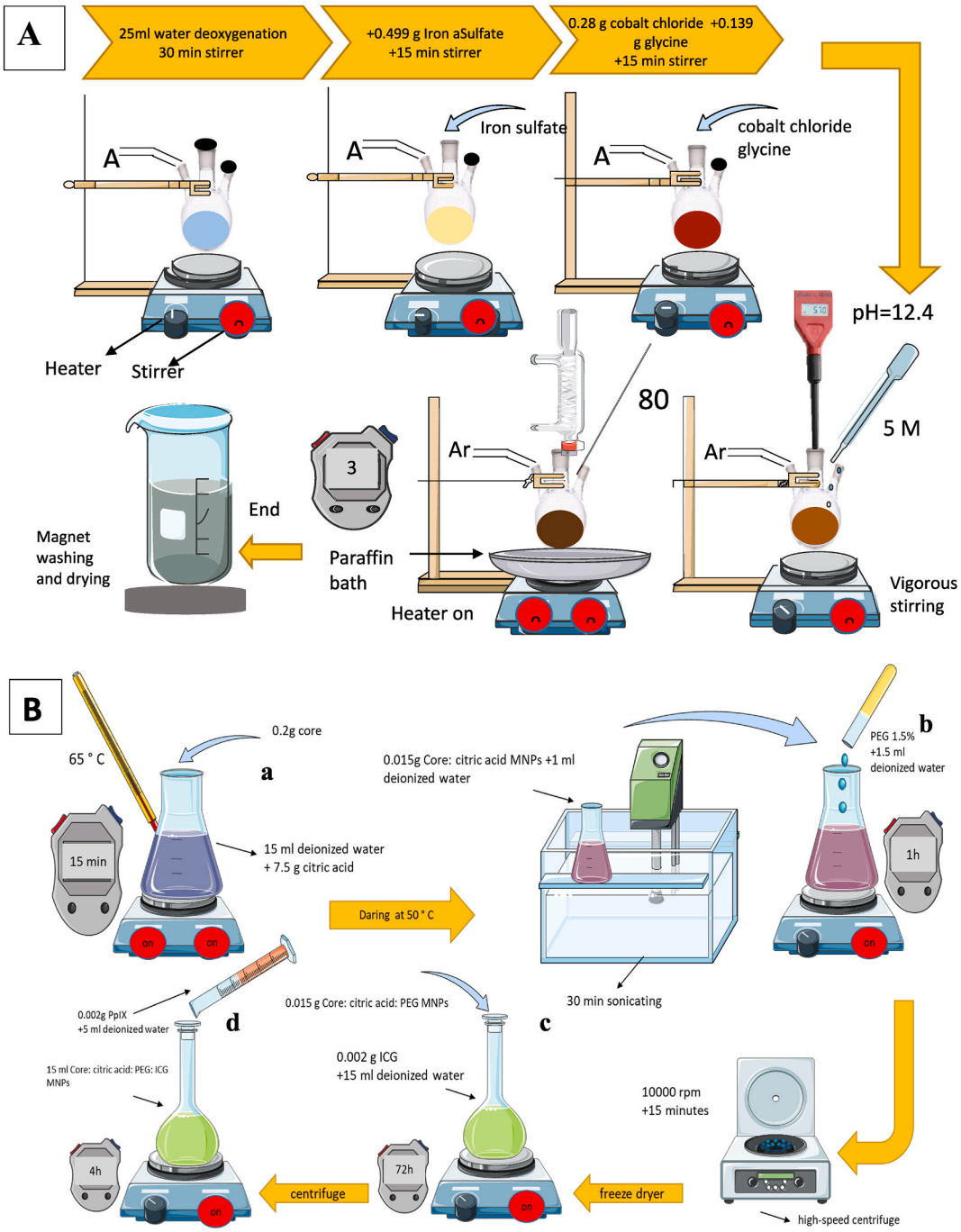

Fig. 1. A) Schematic diagram of the steps of synthesis of Core MNPs. B) Schematic view of the steps of coating and loading sensitizers: a) Preparation of Core: citric acid MNPs. b) Preparation of Core: citric acid: PEG MNPs. c) Preparation of Core: citric acid: PEG: ICG MNPs. d) Preparation of Core: citric acid: PEG: ICG: PpIX MNPs.

anti-human CD133 were belong to Biolegend [33].

2.2. Cell culture

Human skin cancer cell line (A375 cultured in DMED medium) and human breast cancer cell line (MDA-MB-231 cultured in RPMI 1640) were selected for this study. Both cell lines are kept humidified air at 37 °C (5% CO2). The reason for choosing these cell lines is their high metastasis ability. MDA-MB-231 cell line is a triple negative cancer cell line that does not respond to hormonal treatments. Studies have shown that the more aggressive tumor is the one with the higher percentage of CSCs. Studies showed that MDA-MB-231 cell line contained ~79.5% CD44 + $CD24^{-}$cells [34].

2.3. Preparation of cobalt ferrite (core) MNPs

It should be noted that this nanoparticle was synthesized in our previous article, but here we will mention the full details of each step. 25 ml of deionized water was immersed in a three-mouth balloon for half an hour under argon flux. Iron sulfate weighing 0.499 g was added to the water simultaneously with the application of argon flux. After 15min, 0.28 g of cobalt chloride were added to the solution. After another 15min, NaOH was gently added to the solution at a very low rate to reach the pH of 12.4 while stirring vigorously. The entire system was then placed in a paraffin bath and heated to 80°. The resulting cobalt ferrite nanoparticle sediment was washed three times and dried in an oven [33,35](Fig. 1A).

2.4. Preparation of Core: citric acid MNPs

For this purpose, citric acid powder (7.5 g) was weighed and was dissolved in 15 ml of deionized water to obtain a clear solution. Then 0.2 g of core MNPs synthesized from the previous step was added solution. The solution was placed on a stirrer (15 min at 65 °C). Finally, the resulting solution was washed 3 times with deionized water and dried immediately at 50 °C (Fig. 1B a) [33].

2.5. Preparation of Core: citric acid: PEG MNPs

In order to coat the cobalt ferrite core with polyethylene glycol, the following procedure was carried out. Firstly, 1.5% PEG was dissolved in 1.5 ml of deionized water. Next, 0.015 g of cobalt ferrite nanoparticles that were previously coated with citric acid liquefied in deionized water (1 ml), and was placed in ultrasonic bath for 30min until a uniform solution was obtained. The solution was then taken out of the sonicate bath and placed on a high-speed stirrer (with the heater off). At this point, the PEG solution that had been previously prepared was added all at once and the entire solution was stirred on a high-speed stirrer for 1 h. Finally, the resulting solution was centrifuged twice using a high-speed centrifuge (at 10000 rpm for 15min each time) and the last product was dehydrated using a freeze dryer [33,36] (Fig. 1B b).

2.6. Synthesis of core: citric acid: PEG: ICG MNPs

To load ICG on Core: citric acid: PEG MNPs, first, 0.002 g of ICG was dissolved in 15 ml of deionized water. Next, 0.15 g of Core: citric acid: PEG MNPs was added to the solution. The solution was foiled and placed on a magneto stirrer for 24, 48, and 72h. Based on the UV–visible curve, it was determined that the optimal time to keep the solution on the magneto stirrer was 72h. After that, the solution was centrifuged twice (at 10,000 rpm for 15min each time) to eliminate unbound ICG and remove the supernatant (Fig. 1B c) [33].

2.7. Synthesis of core: citric acid: PEG: ICG: PpIX MNPs

The process for conjugating PpIX onto Core: citric acid: PEG: ICG: MNPs involved several steps. Firstly, PpIX (0.002 g) was dissolved in 5 ml of deionized water. Next, the previously prepared nanoparticles loaded with ICG were dissolved in 15 ml of deionized water and added to the PpIX solution. The mixture was then covered with aluminum foil and placed on a medium-speed magnetic stirrer at room temperature for 24, 48, and 72h. The optimal stirring time of 4h was determined based on the UV–visible curve. Finally, after 4h, the loaded nanostructure was washed twice by centrifugation (15min, 10000 rpm) to remove any unbound PpIX (Fig. 1B d). [33].

2.8. Characterization

2.8.1. Diffraction light scattering (DLS)

Poly disparity index (PDI (, hydrodynamic size distribution, and zeta potential of magnetic nanostructures in three stages of synthesis were recorded by DLS device [33].

2.8.2. Transmission electron microscopy (TEM)

Size distribution and Morphology of nanoparticle estimate by TEM. The average size of nanoparticles was estimated from HRTEM histogram of Core MNP in our pervious study [35]. In this study TEM was prepared from final nanostructure in 100 kV field [33].

2.8.3. Scanning electron microscopy (SEM)

Surface structure assesses by SEM. Condition to evaluate NP in SEM was 20 kV High Voltage MIRA3 TESCAN in 1.38 μm of the field of view. SEM was used for Core: citric acid: PEG: ICG: PpIX MNPs and its size distribution was defined by using the SEM image through ImageJ software. SEM of Core MNP was done in our pervious study [33,35].

2.8.4. X-ray diffraction (XRD)

The X-ray diffraction (XRD) is a good way to evaluate crystal lattice structures of NP. Measurement was done in room temperature with an X-ray diffractometer. This measurement was acquired at temperature of 550 °C and condition of 40 kV and 30 mA in a 2θ range of 20°–80° was used in our pervious study [33,35].

2.8.5. Vibrational sample magnetometer (VSM)

Analysis of magnetic materials by VSM device is the main method to study the magnetic attributes of materials. The consequence of this analysis is obtaining the hysteresis curve or the material's hysteresis loop. According to the examination of the VSM curve of Core MNP and the knowledge of the existence of superparamagnetic properties of nanoparticles produced in the previous study [35], in this study, after coating Core MNP with citric acid and PEG in each step, VSM diagrams of the created nanostructure were prepared using superconducting quantum interference device (SQUID) magnetic system [33].

2.8.6. Fourier-transform IR (FTIR)

FTIR spectroscopy Nicolet T model AVATAR 370 FT-IR was used to confirm the attachment of different coverings layers to nanoparticles and to recognize associated functional groups. FTIR was performed for Core: citric acid MNPs and Core: citric acid: PEG MNPs. FTIR of Core MNP was done in our pervious study [33,35].

2.8.7. UV–visible spectroscopy

UV–visible spectrophotometer was used to evaluate the loaded ICG and PpIX optical sensitizers. The percentage of ICG loading in the nanostructure was obtained from the ratio of the absorbance difference of the ICG stock and the supernatant acquired from centrifuging Core: citric acid: PEG: ICG MNPs at the wavelength corresponding to the ICG peak, and the percentage of PpIX loading in the nanostructure was obtained from the ratio of the absorbance difference of the PpIX stock and the supernatant achieved from centrifuging Core: citric acid: PEG: ICG: PpIX MNPs at 630 nm [33].

2.8.8. Spectrofluorometric

In order to determine certain loading of the sensitizer in the nanostructure, the emission spectrum was also prepared by a spectrofluorimeter. In this method, since the emission spectrum of the ICG sensitizer is outside the visible range, it was only used to investigate PpIX. Therefore, PpIX stock and the supernatant obtained from centrifuging Core: citric acid: PEG: ICG: PpIX MNPs was excited at 404 nm and its emission was recorded in the range of 460–700 nm [33].

2.9. Magnetic hyperthermia experiments in the water medium

2.9.1. Heat efficiency of nanoparticles in a magnetic field

Samples contain different groups of nanoparticles (Core: citric acid MNPs, Core: citric acid: PEG MNPs, Core: citric acid: PEG: ICG: PpIX MNPs) with 5 concentrations prepared in 2 ml microtubes. A magnetic hyperthermia system with a frequency of 425 kHz (B = 33.5 mT, P = 4.27 kW) was used to apply heat. microtubes contain nanostructures, were irradiated with alternating field inside the coil of the hyperthermia system for 6 min. Temperature variations curves against time were performed using a fibrous thermometer equipped with OPTILINK software.

2.9.2. ROS production by nanoparticles in magnetic field

To monitor hydroxyl free radicals produced in aqueous medium during magnetic hyperthermia, Terephthalic acid was used as a chemical dosimeter. For this purpose, 13.2 g of Terephthalic was dissolved in 20 ml of water and 0.2 ml of sodium hydroxide 1 M was added to it. Aluminum foil was stretched around the material and placed on the stirrer for 6h. Then Core: citric acid: PEG: ICG: PpIX MNPs with concentrations of 0.02 mg/ml that was prepared with Terephthalic acid. The samples were placed in a MF with a frequency of 425 kHz (B = 33.5 mT, P = 4.27 kW) for 6 and 3 min. The pre-irradiation and post-irradiation magnetic field samples (Core: citric acid: PEG: ICG: PpIX MNPs + Terephthalic acid and Terephthalic acid) were stimulated in a spectrofluorimeter at 310 nm and the emission spectrum was recorded at 420 nm.

2.10. Cytotoxicity of nanoparticles

Two cell lines of MAD-MB-231and A375were seeded at a density of 8000 and 10000 cells/well in a plate and they were incubated at 7 concentrations of the nanostructure. So, MTT assay was performed to define the cell death percentage. Result of cytotoxicity of nanoparticle are in our pervious study [33].

2.11. Physical treatments

To perform the treatments, 400,000 cells for the MDA-MB-231 cell line and 450,000 cells A375 cell line per 35 mm Petri dish were seeded and placed in cell incubator for 24h.Then The cells underwent the next treatments. Finally, the treatments efficacy for A375 and MDA-MB-231 cells respectively after 48 and 24h was determined by MTT assay.

2.11.1. Magnetic hyperthermia protocol

After determining the toxicity of the nanostructures synthesized the optimal concentrations were selected for MHT. After 24hincubation by different nanoparticles the treatment of MHT with nanoparticles and without nanoparticles at frequency of 425 kHz (B = 33.5 mT, P = 4.27 Kw) for 1–6 min in the presence of the Core: citric acid: PEG: ICG: PpIX MNPs and MF duration of 0 and 5min for Core: citric acid MNPs and Core: citric acid: PEG MNPs. The temperature of the Petri dishes was measured by a thermovision camera.

2.11.2. Magnetic hyperthermia with photodynamic therapy

The cells were treated with nanoparticles including Core: citric acid MNPs, Core: citric acid: PEG MNPs and Core: citric acid: PEG: ICG: PpIX MNPs at the concentration obtained by the toxicity test. After 24h incubation, MHT was performed at resonance frequency of 425 kHz (B = 33.5 mT, P = 4.27 Kw). After that, the Petri dish was exposed to LED light source at 630 nm (P = 1 W and I = 7.25 mW/cm2) with the times mentioned in Table 1 and Table 2.

2.11.3. Magnetic hyperthermia with photothermal therapy

The cells were treated with synthesized nanoparticles including Core: citric acid MNPs, Core: citric acid: PEG MNPs and Core: citric acid: PEG: ICG: PpIX MNPs. After 24h incubation, PTT was followed by MHT. The characteristics of the magnetic field used were similar to the previous treatment but here LED of 850 nm (P = 3 W and I = 44.25 mW/cm2) was used. Exposure times and concentration of Core: citric acid: PEG: ICG: PpIX MNPs was the same as Tables 1 and 2 for each cell line.

2.11.4. Combination of hyperthermia, photodynamic and photothermal treatments

In this combined treatment, petri dishes were seeded with the specified concentration and incubated with Core: citric acid MNPs, Core: citric acid: PEG MNPs and Core: citric acid: PEG: ICG: PpIX MNPs with a specified concentration for 24h. Then magnetic hyperthermia with the specified conditions was applied. After applying the magnetic field, the Petri dishes were irradiated to LED of 630 nm and 850 nm simultaneous. The characteristics of the magnetic field and light sources were mentioned above. The concentration and Exposure times are similar to Table 1 and Table 2 for each cell line.

2.12. Flow cytometry analysis

First, MDA-MB-231 and A375 cell lines with density of 400,000 cells and 450,000 cells, respectively were seeded and incubated with Core: citric acid: PEG: ICG: PpIX MNPs at a IC20 for both cell line in 35 mm petri dishes for 24 h. Then, all treatment groups (MHT, MHT + PDT, MHT + PTT, MHT + PDT + PTT) were treated in above mentioned treatment conditions. After trypsinization and washing twice with 20% FBS, 10^6 cells were poured into each flow cytometry tube. Then, 2.5 μL of each conjugated antibodies (CD133, CD44, and CD24 were added to cell containing tubes. After 30 min incubation with antibodies, cells were washed to eliminate the unbound antibodies. Finally, the results were recorded using a flow cytometer (FACSCalibur, BD, USA).

2.13. Evaluation indexes

2.13.1. IC20 index

It is a concentration of nanoparticles that causes 20% cell death, which was achieved by MTT assay. Our experiments were done with this concentration [33].

2.13.2. Combinational Indices (CIs)

In order to compare the efficacy of the treatments, CIs was defined to compare the groups. For this purpose, the synergistic effects of different treatments with and without drugs were calculated for each cell line. In this way, if three factors A, B and C affect cell survival separately or in combination with each other, the CIs are defined as follows:

$$\text{Combinational Indices (CIs)} = \frac{VA \times VB \times VC}{VABC}$$

Table 1
Concentration (mg/ml), LED radiation (min), magnetic field apply duration (MDA-MB-231).

Groups	Concentration (mg/ml)	LED time exposure (min)	magnetic field apply duration (min)
Control	0–0.05	0-1-3-5	0-1-3
Core: citric acid MNPs	0–0.05	0.5	0–3
Core: citric acid: PEG MNPs	0–0.05	0.5	0–3
Core: citric acid: PEG: ICG: PpIX MNPs	0–0.05	0-1-3-5	0-1-3

Table 2
Concentration (mg/ml), LED radiation (min), magnetic field apply duration (A375).

Groups	Concentration (mg/ml)	LED time exposure (min)	magnetic field apply duration (min)
Control	0–0.025	0-1-3-5	0-1-3
Core: citric acid MNPs	0–0.025	0.5	0–3
Core: citric acid: PEG MNPs	0–0.025	0.5	0–3
Core: citric acid: PEG: ICG: PpIX MNPs	0–0.025	0-1-3-5	0-1-3

Here, V_A, V_B, V_C are the cell survival under the separate effects of factors A, B and C. while V_{ABC} is survival of their simultaneous combination. In this index, values greater than one, equal to one, and less than one indicate the cooperation effect, synergy effect, and opposite effect of factors A, B, and C, respectively [37].

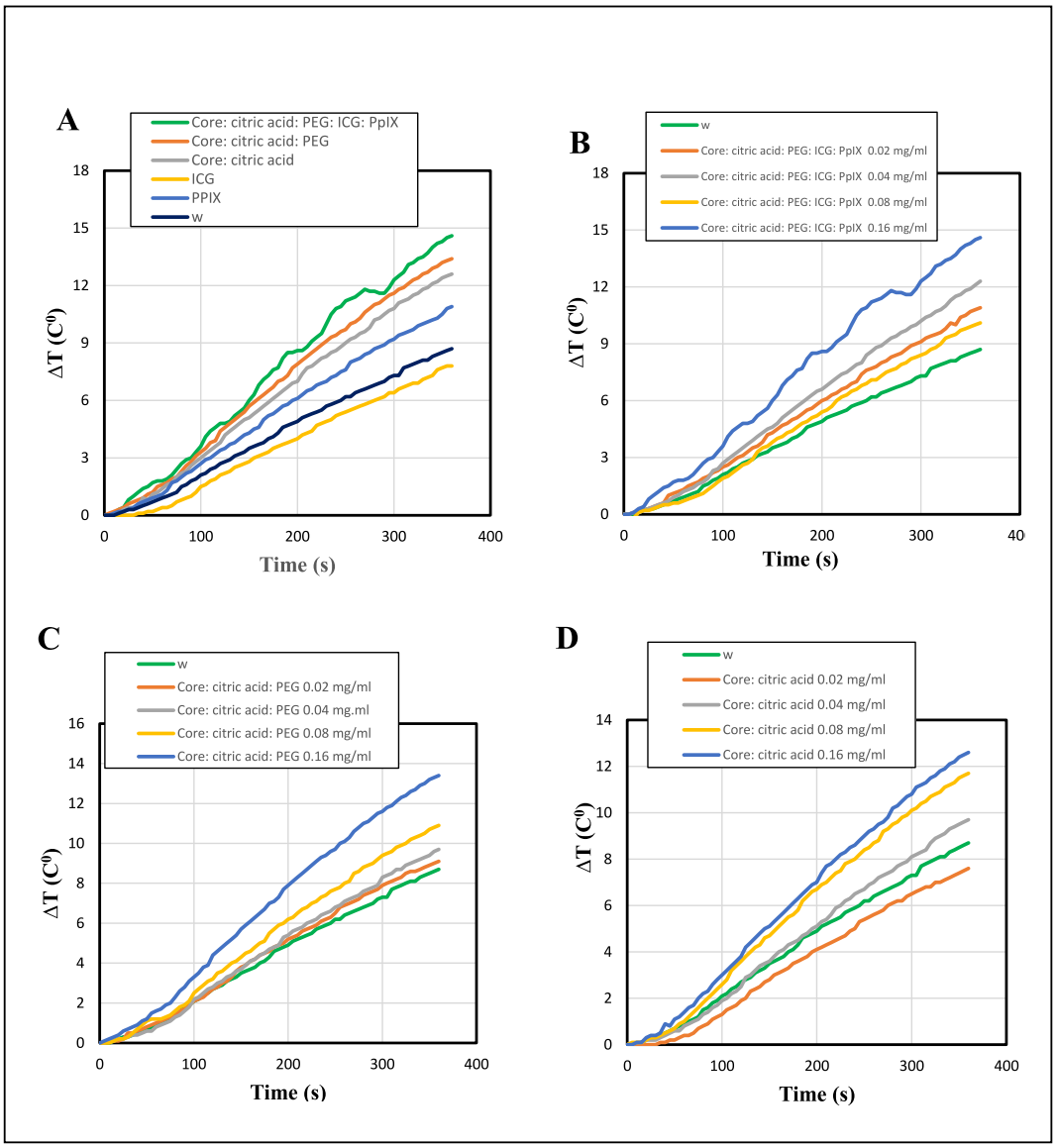

Fig. 2. A) temperature changes of nanostructures include Core: citric acid MNPs, Core: citric acid: PEG MNPs, Core: citric acid: PEG: ICG: PpIX MNPs, ICG and PpIX at a concentration of 0.16 mg/ml. B) Core: citric acid: PEG: ICG: PpIX MNPs temperature changes in different concentrations. C)Graph of temperature changes of Core: citric acid: PEG MNPs in different concentrations. D) Graph of temperature changes of Core: citric acid MNPs in different concentrations. (f = 425 kHz, B = 33.5 mT, P = 4.27 kW, time = 0–6 min).

2.13.3. Statistical analysis

Normality of data checked with Kolmogorov-Smirnov test (k-s test). Then, Tukey's test and One-way ANOVA analysis of variance were used in statistical software SPSS23 to compare the data with a confidence level of 95%.

3. Results

3.1. Characterization of MNPs

Characteristics of synthesized nanoparticles, parameters such as hydrodynamic size, zeta potential, conductivity, and poly disparity index of nanoparticles was measured by DLS and reported in our pervious study [33]. The size of Core MNPs was evaluated in our pervious study by HRTEM image and it was about 10.45 nm. The shape of Core MNPs estimated to be amorphous [35]. TEM image and SEM image of Core: citric acid: PEG: ICG: PpIX MNPs are shown in our previous study. Average size of Core: citric acid: PEG: ICG: PpIX MNPs was determined by its histogram of SEM image and estimated about 13 nm, which was carried by ImageJ software [33]. By investigation of the VSM curve in our pervious study superparamagnetic properties of Core MNPs were confirmed [35]. VSM curve of Core: citric acid MNPs, and VSM curve of Core: citric acid: PEG: ICG: PpIX MNPs, which was evaluated using the SQUID magnetic system. According to the VSM curves obtained from our perviouse study, none of the Core MNPs, Core: citric acid MNPs, and Core: citric acid: PEG MNPs reached saturation magnetization. These VSM curves shows the no hysteresis loop of these nanoparticles [33]. FTIR of Core: citric acid MNPs and Core: citric acid: PEG MNPs, obtained in the range of 4000–500. This graphs were prepared to ensure proper coating and connection of citric acid and PEG to Core MNPs. There are peaks in region of 3500–2800, 1580.63 and 1343 are related to Core: citric acid MNPs FTIR and peaks in the region of 3418.85 and 2872.24 are related to Core: citric acid: PEG MNPs FTIR [33]. Absorption spectrum of ICG stock and supernatant related to Core: citric acid: PEG: ICG MNPs phase were prepared in our pervious study, in which indications that the loading percentage of ICG in the nanostructure is 60.4%. Also absorption spectrum of PpIX stock and supernatant related to Core: citric acid: PEG: ICG: PpIX MNPs phase demonstrates the loading percentage of PpIX in the nanostructure is 84.64% [33]. Stability of nanoparticles was measured both with DLS and UV–visible spectrophotometer in our pervious study [33]. According to that data Core: citric acid: PEG: ICG: PpIX MNPs was stable it shows no loss of absorption peak after one month [33].

3.2. Magnetic hyperthermia studies in the water medium

3.2.1. Heat efficiency of nanoparticles in a magnetic field

Fig. 2A demonstrates temperature changes of nanostructures include Core: citric acid MNPs, Core: citric acid: PEG MNPs, Core: citric acid: PEG: ICG: PpIX MNPs, ICG and PpIX at a concentration of 0.16 mg/ml. It shows highest temperature change is belonging to Core: citric acid: PEG: ICG: PpIX MNPs (ΔT~15C°) then Core: citric acid: PEG MNPs (ΔT~13.4C°), Core: citric acid MNPs (ΔT~12.6C°), PpIX (ΔT~10.9C°), water (ΔT~8.6C°) and ICG (ΔT~7.8C°), respectively. Fig. 2B shows Core: citric acid: PEG: ICG: PpIX MNPs temperature changes in concentrations of 0, 0.02, 0.04, 0.08, 0.16 mg/ml. According to this graph as the concentration increases, temperature changes increase. Fig. 2C shows temperature changes of Core: citric acid: PEG MNPs in concentrations of 0,

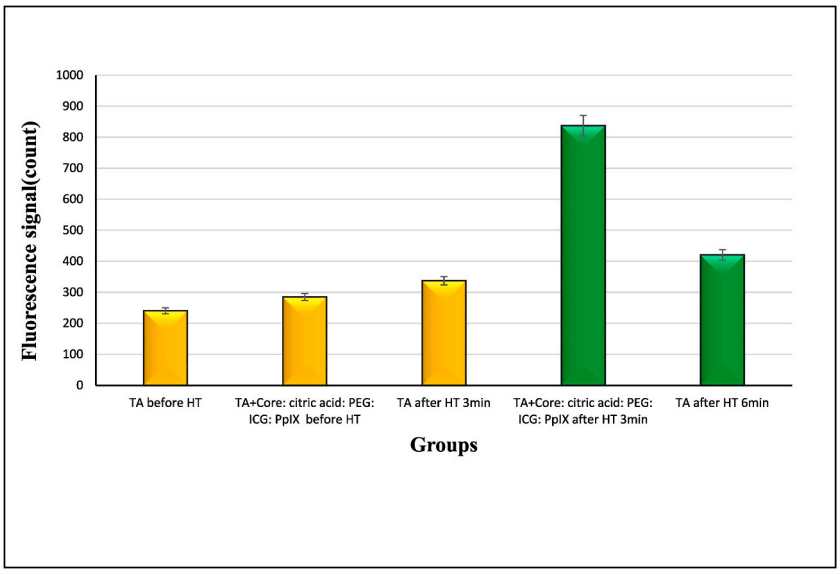

Fig. 3. Spectrofluorimeter diagram of Terephthalic acid and Terephthalic acid with a concentration of 0.02 mg/ml Core: citric acid: PEG: ICG: PpIX MNPs under magnetic field (f = 425 kHz, B = 33.5 mT, P = 4.27 kW, time = 3 and 6 min).

0.02, 0.04, 0.08, 0.16 mg/ml which indicates that by increasing concentration, temperature changes rise. Fig. 2D demonstrations temperature changes of Core: citric acid MNPs in concentrations of 0, 0.02, 0.04,0.08,0.16 mg/ml so it also confirms temperature change has correlation with concentration, high concentration brings high temperature changes. All experiment related to Fig. 2 prepared under magnetic field with a frequency of 425 kHz (B = 33.5 mT, P = 4.27 kW, and t = 6 min).

3.2.2. ROS production of nanoparticle in magnetic field

Fig. 3 shows spectrofluorimeter diagram of Terephthalic acid and Terephthalic acid with a concentration of 0.02 mg/ml Core: citric acid: PEG: ICG: PpIX MNPs under magnetic field with frequency of 425 kHz (B = 33.5 mT, P = 4.27 kW) for 6 and 3 min. It shows that with the increase in time duration of magnetic field, the emission intensity of Terephthalic acid and Core: citric acid: PEG: ICG: PpIX MNPs increases. which is proof of the production of hydroxyl radicals is depends on the time of applying the magnetic field.

3.3. Cytotoxicity of nanoparticles

Cytotoxicity of these MNPs in different concentration evaluated for both cell line in our pervious study. According to cell survival

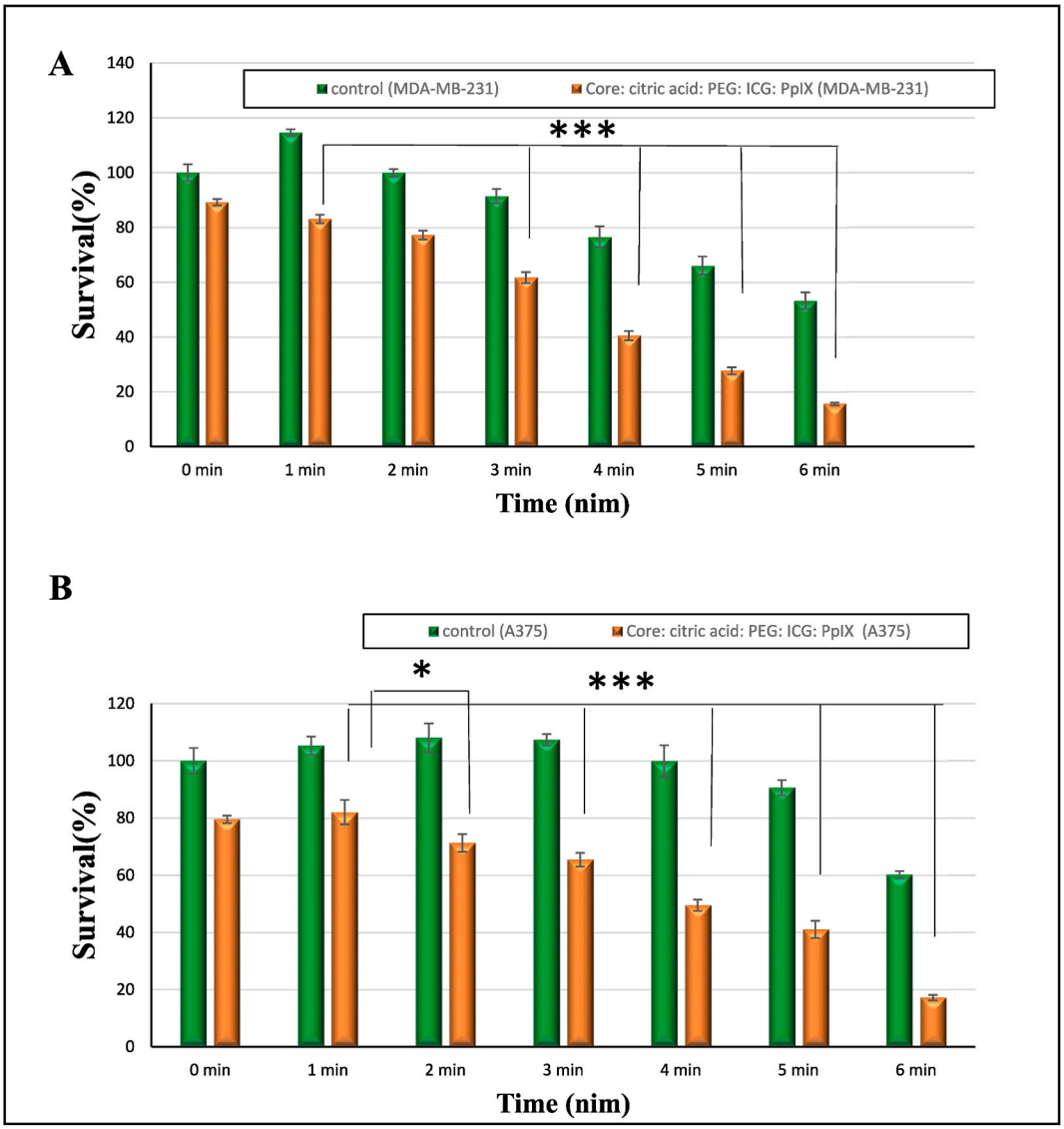

Fig. 4. A) Comparison of cell survival changes between the control and Core: citric acid: PEG: ICG: PpIX MNPs groups at a concentration of 0.05 mg/ml Core: citric acid: PEG: ICG: PpIX MNPs in the MDA-MB-231 cell line. B) Comparison of cell survival changes between the control and Core: citric acid: PEG: ICG: PpIX MNPs groups at a concentration of 0.025 mg/ml Core: citric acid: PEG: ICG: PpIX MNPs in the A375 cell line. (f = 425 kHz, B = 33.5 mT, P = 4.27 kW, time = 0–6 min).

cure IC20 for MAD-MB-231 cell line is 0.05 mg/ml and for A375 cell line is 0.025 mg/ml [33].

3.4. Magnetic hyperthermia (MHT)

Fig. 4A and B shows comparison of cell survival changes between the control and Core: citric acid: PEG: ICG: PpIX MNPs groups at a

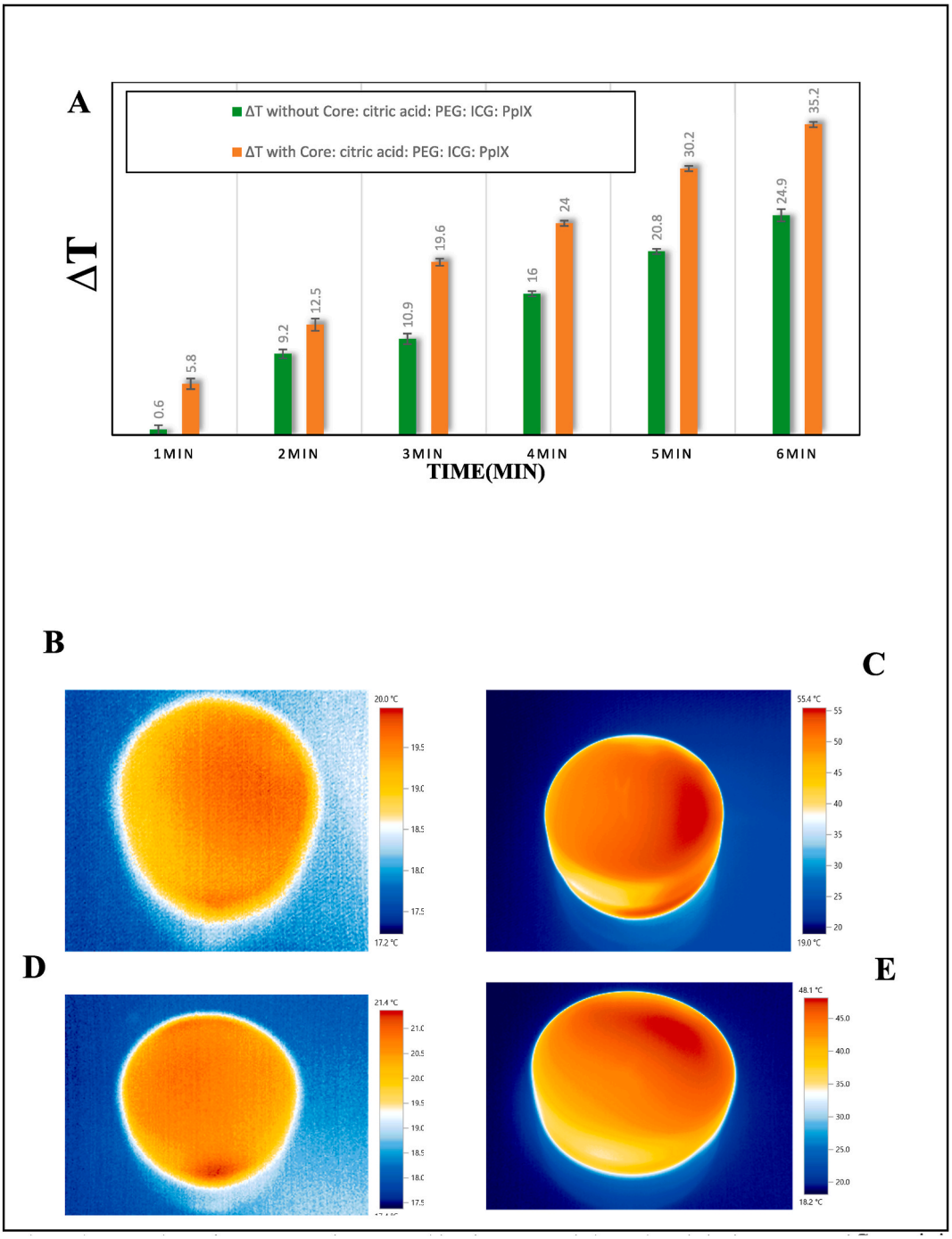

Fig. 5. A) Comparison of temperature changes resulting from magnetic hyperthermia in the presence of Core: citric acid: PEG: ICG: PpIX MNPs with a concentration of 0.025 mg/ml and control group in the cell environment due to the application of a magnetic field in 1–6 min (f = 425 kHz, B = 33.5 mT, P = 4.27 kW). B) and C) Temperature image before and after applying magnetic hyperthermia for 6 min in Core: citric acid: PEG: ICG: PpIX MNPs group. D) and E) Temperature image before and after applying magnetic hyperthermia for 6 min in control group.

concentration of 0.05 mg/ml Core: citric acid: PEG: ICG: PpIX MNPs in the MDA-MB-231 cell line and concentration of 0.025 mg/ml Core: citric acid: PEG: ICG: PpIX MNPs in the A375 cell line in magnetic field with a frequency of 425 kHz, the intensity of 33.5 mT and the power of4.27 kW in 0–6 min, respectively. In both cell line cell survival decreases with increasing time of applying magnetic field and in both cell lines have significant difference between Core: citric acid: PEG: ICG: PpIX MNPs and control groups (P-value<0.05). Fig. 5A shows comparison of temperature changes resulting from MHT in the presence of Core: citric acid: PEG: ICG: PpIX MNPs with a concentration of 0.025 mg/ml and control group in the cell environment due to the application of a magnetic field with a frequency of 425 kHz (B = 33.5 mT, P = 4.27 kW) in 1–6 min. According to this graph maximum temperature change happens in 6 min of applying of magnetic field to Core: citric acid: PEG: ICG: PpIX MNPs (ΔT = 35.2 °C) then 5 min (ΔT = 30.2 °C), 3 min (ΔT = 24 °C), 2 min (ΔT = 12.5 °C) and 1 min (ΔT = 5.8 °C). Fig. 5B– C Temperature image before and after applying magnetic hyperthermia for 6 min in Core: citric acid: PEG: ICG: PpIX MNPs group and it reach from 20 °C to 55.4 °C. Fig. 5D– E Temperature image before and after applying magnetic hyperthermia for 6 min in control group which reach from 21.4 °C to 48.1 °C.

3.5. Magnetic hyperthermia with photodynamic therapy

Fig. 6A– B compare the cell survival of the control group and Core: citric acid: PEG: ICG: PpIX MNPs with a concentration of 0.05

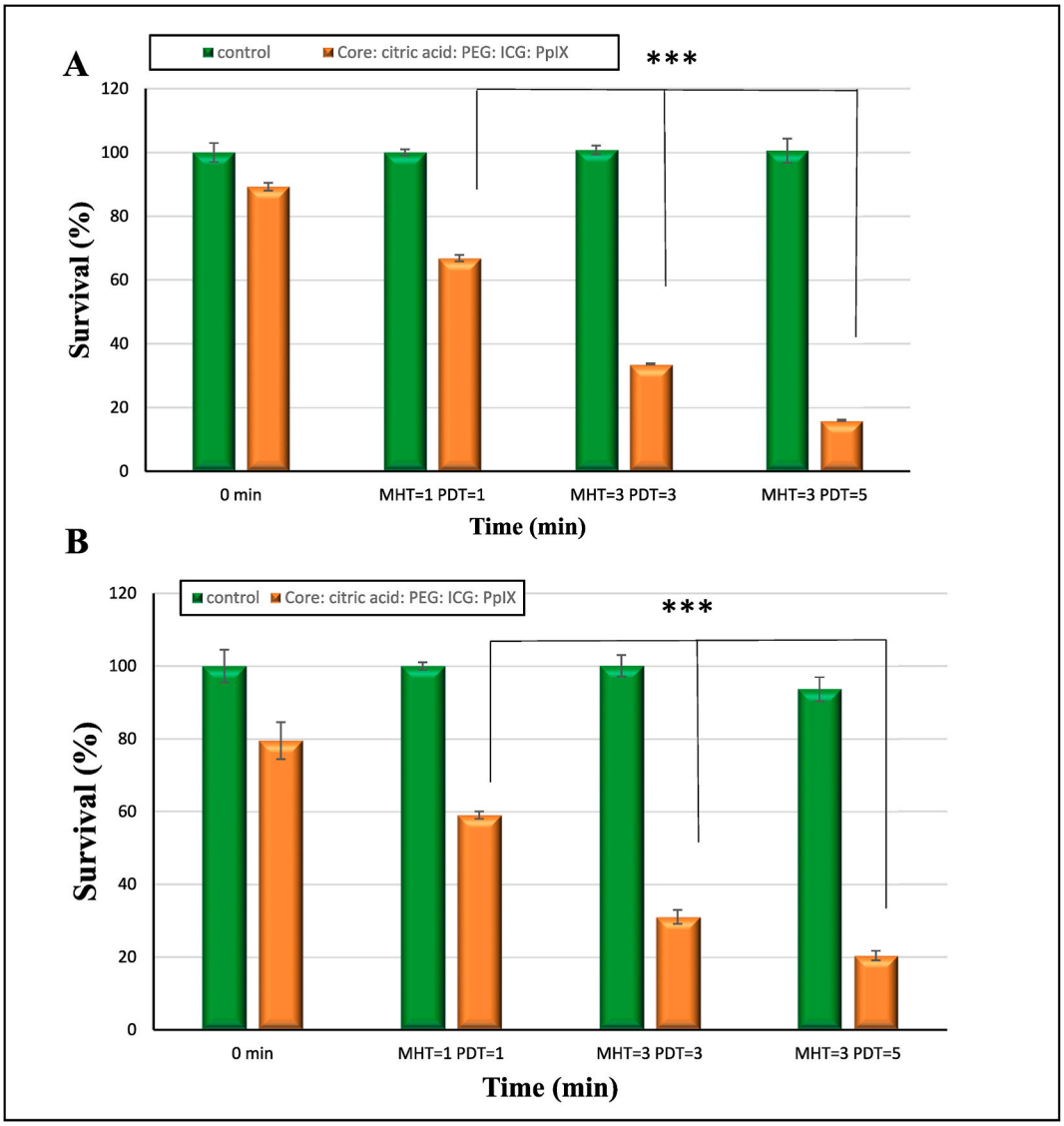

Fig. 6. A) and B) Compartion of cell survival of the control group and Core: citric acid: PEG: ICG: PpIX MNPs with a concentration of 0.05 mg/ml in the MDA-MB-231 cell line and a concentration of 0.025 in the A375 cell line in the combined treatment Magnetic hyperthermia and photodynamic therapy at different treatment times, respectively. (Magnetic hyperthermia/f = 425 kHz, B = 33.5 mT, P = 4.27 kW. Photodynamic therapy/ wavelength = 630 nm, P = 1W, I = 7.25 mW/cm2).

mg/ml in the MDA-MB-231 cell line and a concentration of 0.025 in the A375 cell line in the combined treatment Magnetic hyperthermia and photodynamic therapy at different treatment times, respectively. In both cell lines by increasing time of magnetic field and light exposure, cell survival has significant decrease (P-value<0.001). Fig. 7A– B shows comparison of cell survival between Core: citric acid: PEG MNPs and Core: citric acid: PEG: ICG: PpIX MNPs with a concentration of 0.05 mg/ml in the MDA-MB-231 cell line and a concentration of 0.025 in the A375 cell line in the combined treatment Magnetic hyperthermia and photodynamic therapy, respectively. In both cell lines there is significant decrease in survival between Core: citric acid: PEG: ICG: PpIX MNPs with other groups (Core: citric acid MNPs, Core: citric acid: PEG MNPs) (P-value = 0). In MDA-MB-231 cell line there is major decrease in survival between CoFe2O4@citric and Core: citric acid: PEG MNPs (P-value = 0.01), while there is no noteworthy difference between Core: citric acid MNPs and Core: citric acid: PEG MNPs in A375 cell line (P-value>0.05).

3.6. Magnetic hyperthermia with photothermal therapy

Fig. 8A– B illustrates cell survival of the control group and Core: citric acid: PEG: ICG: PpIX MNPs with a concentration of 0.05 mg/ml in the MDA-MB-231 cell line and a concentration of 0.025 in the A375 cell line in the combined treatment Magnetic hyperthermia

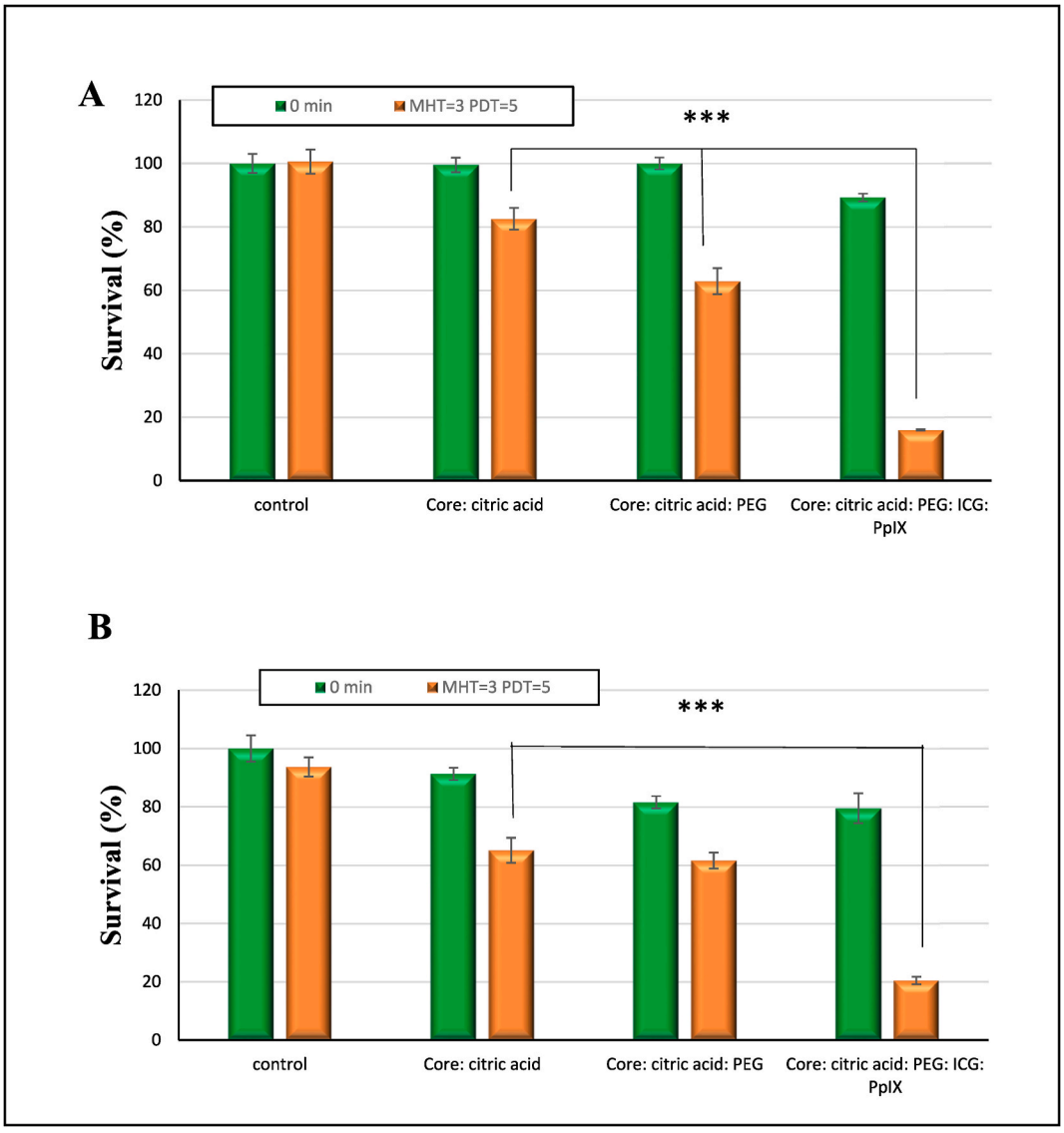

Fig. 7. A) and B) Comparison of cell survival between Core: citric acid MNPs, Core: citric acid: PEG MNPs and Core: citric acid: PEG: ICG: PpIX MNPs with a concentration of 0.05 mg/ml in the MDA-MB-231 cell line and a concentration of 0.025 in the A375 cell line in the combined treatment Magnetic hyperthermia and photodynamic therapy. (Magnetic hyperthermia/f = 425 kHz, B = 33.5 mT, P = 4.27 kW. Photodynamic therapy/wavelength = 630 nm, P = 1W, I = 7.25 mW/cm2).

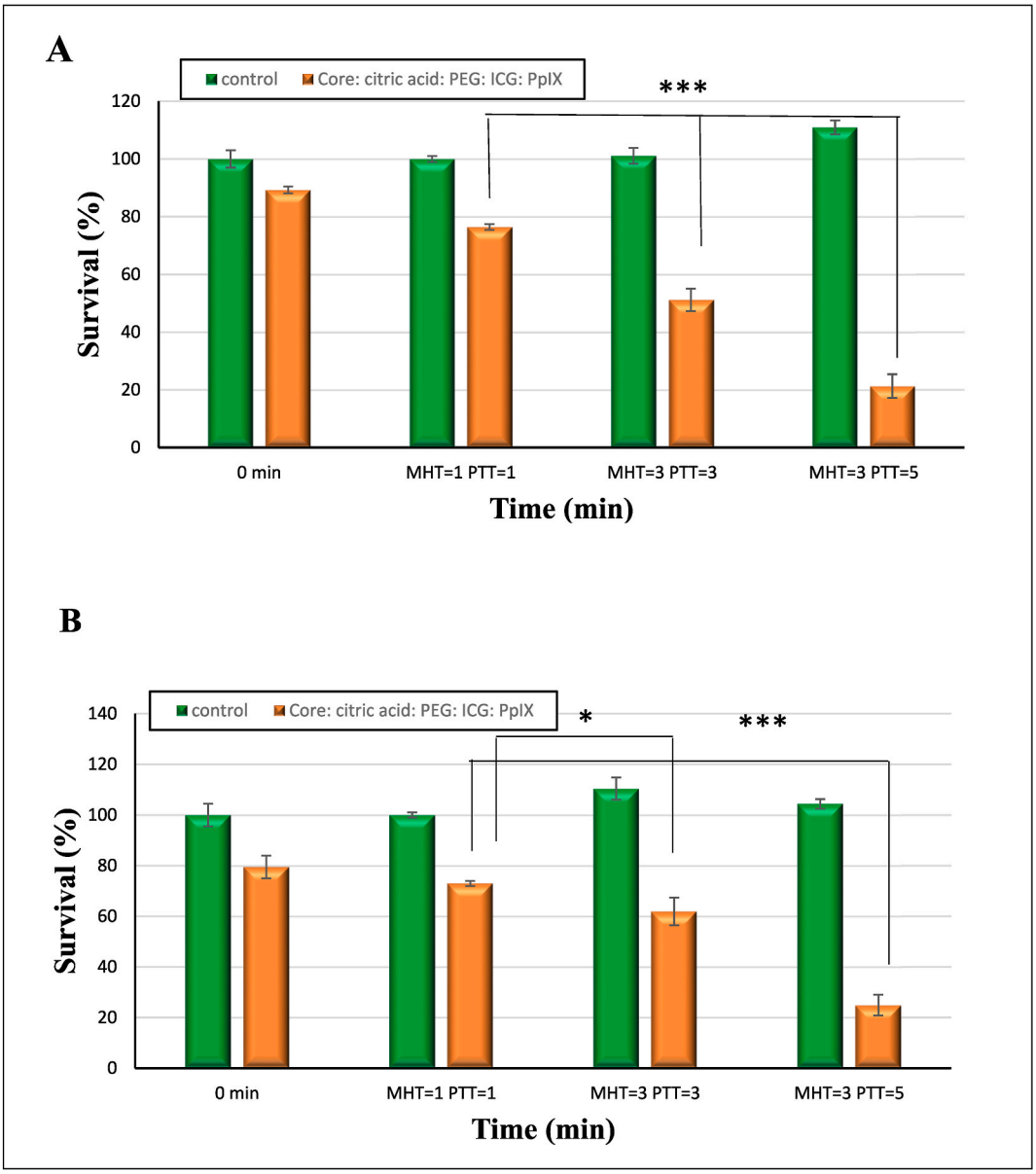

Fig. 8. A) and B) Illustration of cell survival of the control group and Core: citric acid: PEG: ICG: PpIX MNPs with a concentration of 0.05 mg/ml in the MDA-MB-231 cell line and a concentration of 0.025 in the A375 cell line in the combined treatment Magnetic hyperthermia and photothermal therapy at different treatment times, respectively. (Magnetic hyperthermia/f = 425 kHz, B = 33.5 mT, P = 4.27 kW. Photothermal therapy/ wavelength = 850 nm, P = 3W, I = 44.25 mW/cm2).

and photothermal therapy at different treatment times, respectively. In general, it shows the logical relationship between survival reduction and exposure times in both cell lines. In both cell line by increasing exposure time, survival drop down. There is significant difference between Core: citric acid: PEG: ICG: PpIX MNPs (MHT = 3 PTT = 5) with other exposure times (P-value = 0) but between Core: citric acid: PEG: ICG: PpIX MNPs (MHT = 3 PTT = 3) and Core: citric acid: PEG: ICG: PpIX MNPs (MHT = 1 PTT = 1) groups just in MDA-MB-231 cell line there is noticeable difference (P-value<0.05). According to Fig. 9A– B in both cell line there is a major reduction in survival between Core: citric acid: PEG: ICG: PpIX MNPs with other groups (Core: citric acid MNPs, Core: citric acid: PEG MNPs) (P-value = 0). In MDA-MB-231 cell line there is significant drop in survival between Core: citric acid MNPs and Core: citric acid: PEG MNPs, (P-valve<0.05), while there is no noteworthy difference between these two group in A375 cell line (P-value>0.05).

3.7. Combination of hyperthermia, photodynamic and photothermal treatments

Fig. 10A– B shows the same behaver of these two cell line in response to exposure times. In both cell line with increasing time of LED

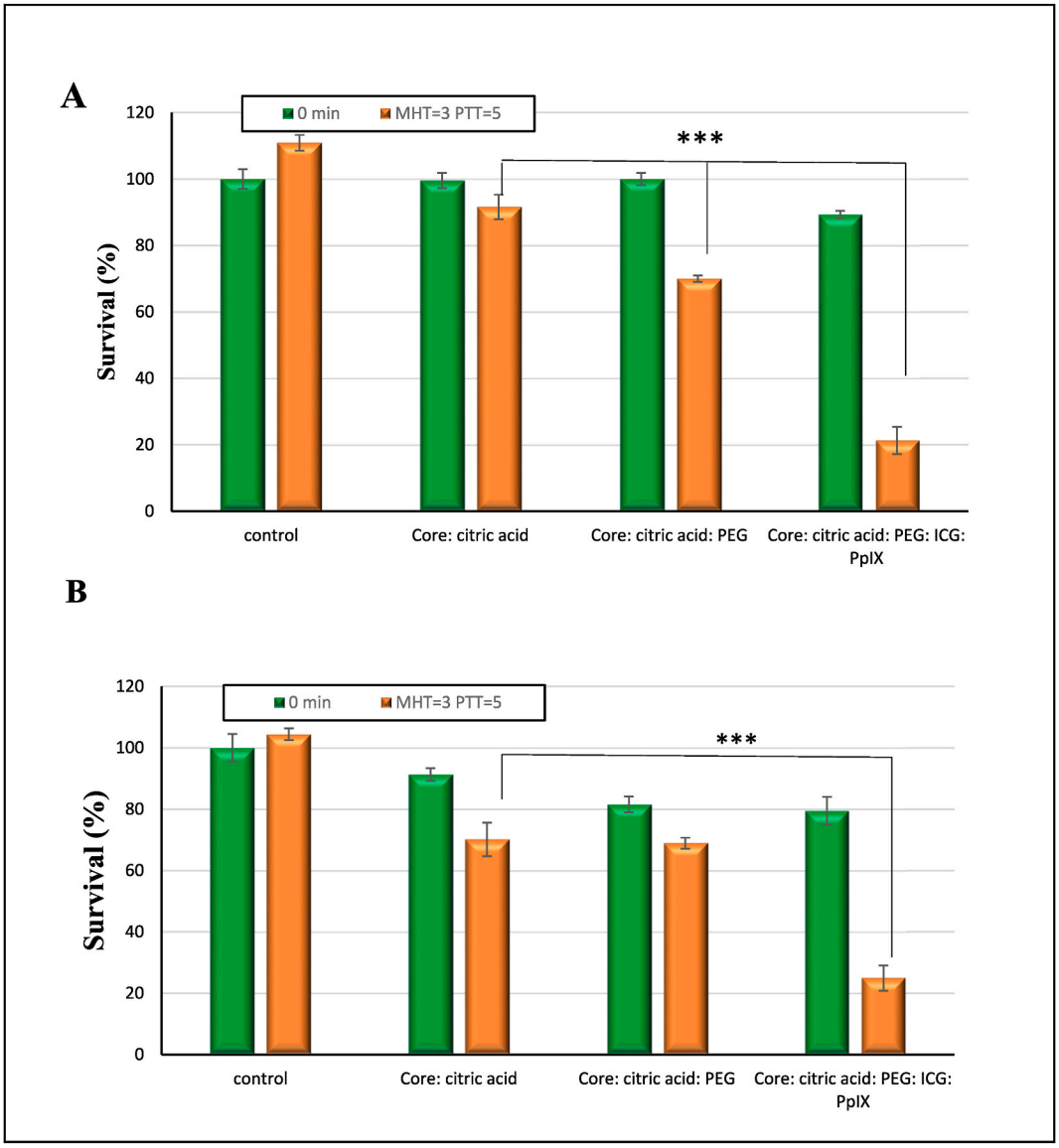

Fig. 9. A) and B) Comparison of cell survival between Core: citric acid MNPs, Core: citric acid: PEG MNPs and Core: citric acid: PEG: ICG: PpIX MNPs with a concentration of 0.05 mg/ml in the MDA-MB-231 cell line and a concentration of 0.025 in the A375 cell line in the combined treatment Magnetic hyperthermia and photothermal therapy. (Magnetic hyperthermia/f = 425 kHz, B = 33.5 mT, P = 4.27 kW. Photothermal therapy/ wavelength = 850 nm, P = 3W, I = 44.25 mW/cm2).

exposure and time of applying magnetic field, survival significantly drops (P-value<0.001). Fig. 11A– B is a comparative graph between Core: citric acid MNPs, Core: citric acid: PEG MNPs and Core: citric acid: PEG: ICG: PpIX MNPs, which shows the high dependence of Core: citric acid: PEG: ICG: PpIX MNPs on the time of light irradiation and application of magnetic field compared to other nanoparticle groups. These difference is noticeable compare to other group of nanoparticles (P-value<0.001). This exposure dependence between Core: citric acid MNPs and Core: citric acid: PEG MNPs in MDA-MB-231 cell line ((P-value<0.001) is more than A375 cell line (P-value<0.05).

3.8. Flow cytometry findings

The final effect of treatment (MHT, MHT + PTT, MHT + PDT and MHT + PDT + PTT) on cancer stem cells in both cell lines were evaluated using monoclonal antibodies like CD24, CD44, and CD133. Figs. 1S and 2S shows follow cytometry image of these MDA-MB-231 and A375 cell lines, respectively, in which CD44 + $CD24^{-}$cells was gated for distinguishing CSCs. Fig. 12A– B displays the result of gating flow cytometry images in the form of a diagram. According to Figs. 12A– B in both cell line MHT + PDT + PTT has good effect on

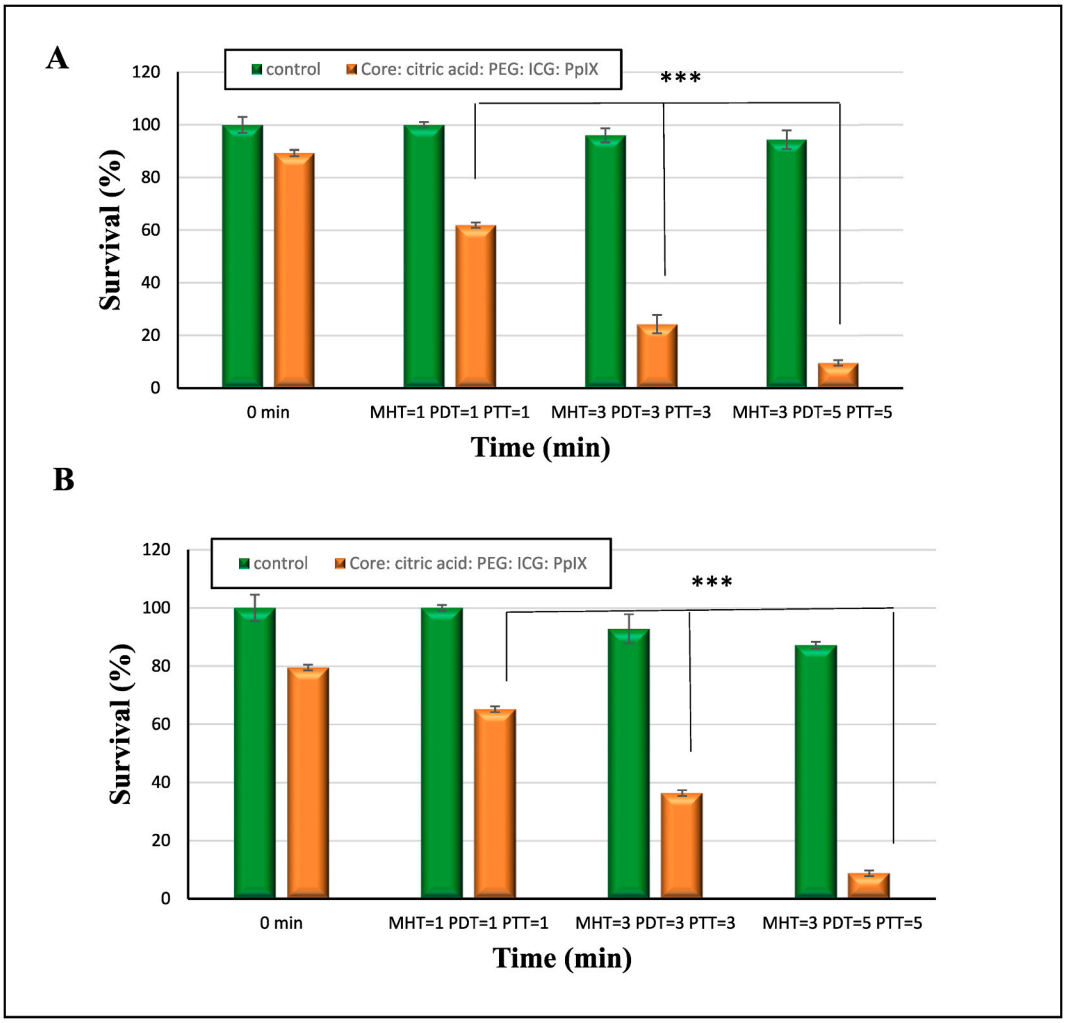

Fig. 10. A) and B) Illustration of cell survival of the control group and Core: citric acid: PEG: ICG: PpIX MNPs with a concentration of 0.05 mg/ml in the MDA-MB-231 cell line and a concentration of 0.025 in the A375 cell line in the combined treatment Magnetic hyperthermia/photothermal therapy/photothermal therapy at different treatment times, respectively. (Magnetic hyperthermia/f = 425 kHz, B = 33.5 mT, P = 4.27 kW. Photodynamic therapy/wavelength = 630 nm, P = 1W, I = 7.25 mW/cm2. Photothermal therapy/wavelength = 850 nm, P = 3W, I = 44.25 mW/cm2).

elimination of CD44 + $CD24^{-}$cells compare to MHT + PTT and MHT + PDT. This reduction is more significant in MHT + PDT + PTT in A375 cell line compare to MDA-MB-231 $A^{37}5$ cell line (P-value<0.001). In Fig. 12A there is a substantial difference between MHT, MHT + PTT, MHT + PDT and MHT + PDT + PTT (P-value<0.001), while Fig. 12B indicate no noticeable difference between MHT + PTT, MHT + PDT. Figs. 3S and 4S shows follow cytometry image of MDA-MB-231 and A375 cell lines, respectively, in which CD133 + $CD44^{+}$ cells were gated for distinguishing CSCs. Fig. 13A– B displays the result of gating flow cytometry images in the form of a diagram. As shown in these two figures cells withCD133 + $CD44^{+}$ markers in MDA-MB-231 and A375 cell lines have good response to MHT + PDT + PTT compare to single treatments. Reduction in cells with CD133 + $CD44^{+}$ markers for A375 cell line is more obvious than MDA-MB-231 cell line. In the MDA-MB-231 cell line, the pile chart consists of 26% control group, 25% drug control, 23% MHT, 11% MHT + PDT,11% MHT + PTT and 4% MHT + PTT + PDT, while in the A375 cell line, the pile chart consists of 40% control group, 35% drug control, 14% MHT, 6% MHT + PDT,4% MHT + PTT and 1% MHT + PTT + PDT, which shows that combination groups had a small share in the pie chart.

3.9. Evaluation indexes

3.9.1. IC20 index

IC20 index was calculated from our pervious study for both cell lines (concentration which kills 20% of cells). IC20 for MDA-MB-231 cell line is 0.05 mg/ml and for A375 is 0.025 mg/ml [33].

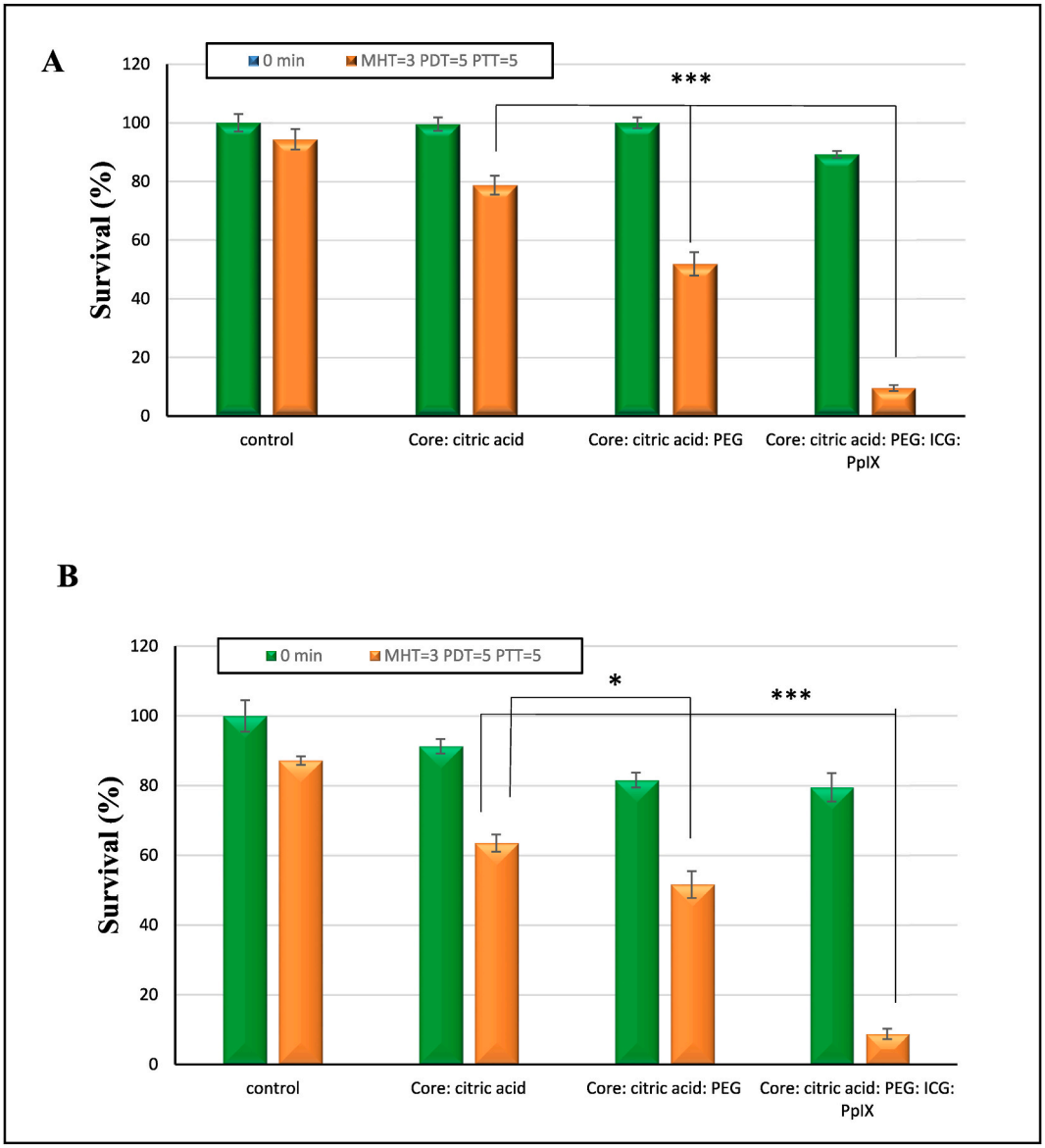

Fig. 11. A) and B) Comparison of cell survival between Core: citric acid MNPs, Core: citric acid: PEG MNPs and Core: citric acid: PEG: ICG: PpIX MNPs with a concentration of 0.05 mg/ml in the MDA-MB-231 cell line and a concentration of 0.025 in the A375 cell line in the combined treatment Magnetic hyperthermia/photothermal therapy/photothermal therapy. (Magnetic hyperthermia/f = 425 kHz, B = 33.5 mT, P = 4.27 kW. Photodynamic therapy/wavelength = 630 nm, P = 1W, I = 7.25 mW/cm2. Photothermal therapy/wavelength = 850 nm, P = 3W, I = 44.25 mW/cm2).

3.9.2. Combination Indices (CIs)

In order to investigate effectiveness of dual and triple combined treatments, combination Indices (CIs) were calculated. The values of CIs for each group are shown in Table 3 and Table 4.

4. Discussion

This study intended to investigate the performance of superparamagnetic Core: citric acid: PEG: ICG: PpIX MNPs nanoparticle as a multifunctional particle for combination therapy of magnetic hyperthermia with photodynamic and photothermal therapy. Another advantage of this nanoparticle is the ability to use it in diagnosis and treatment at the same time. Due to the high atomic number of iron and cobalt that make up and magnetic properties of the core of this nanoparticle, this nanoparticle can be used as a contrast agent in CT scan or MIR.

Choosing the chemical composition and size of MNP is important to control the magnetization of nanoparticles and effectively leads to improving its performance in magnetic hyperthermia. So, co-precipitation method was used for the synthesis of Core: citric acid:

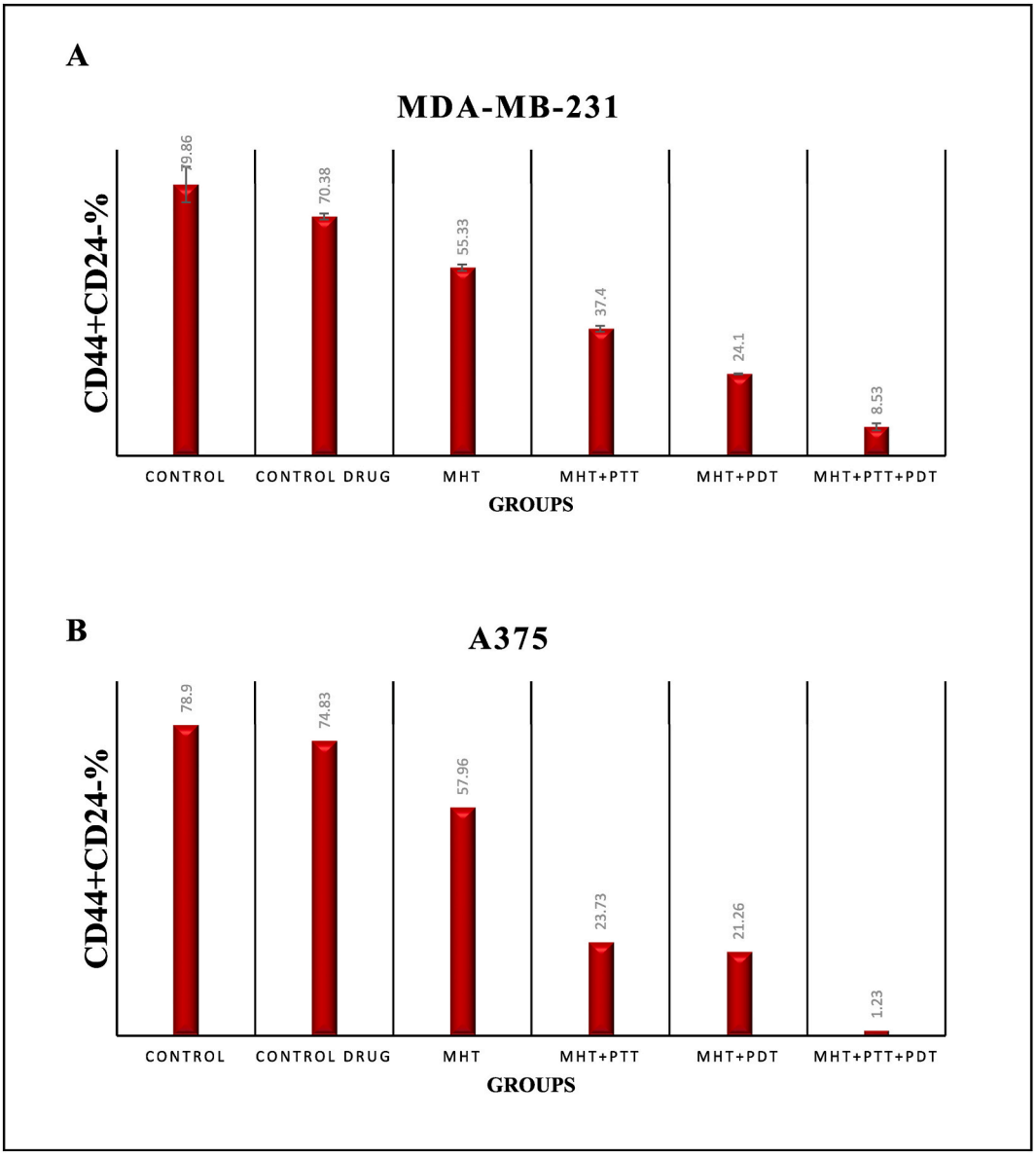

Fig. 12. Flow cytometry analyses. A) Percentage of CD44 + CD24^{-}cell in single or multiple treatments of MDA-MB-231 cell line. B) Percentage of CD44 + CD24^{-}cell in single or multiple treatments of A375 cell line.

PEG: ICG: PpIX MNPs [38].

Factors such as nanoparticle suspension concentration, scattering angle, and isotropy of nanoparticle shape can affect the size obtained from DLS, and the exact and correct size of magnetic nanoparticles cannot be obtained with this method [39]. These MNPs have stable kinetic energy due to their kinetic energy. Since the scattering intensity is directly proportional to the sixth order of the particle radius, this technique is very sensitive to aggregation and is a good method to check the colloidal stability of MNPs suspension [40]. When MNP are coated with materials that are transparent to electrons, for example, in a study where iron oxide nanoparticles were coated with oleic acid and oleylamine acid (completely transparent) the TEM size was smaller than DLS [41,42]. This was also true in our study. DLS of Core MNPs, Core: citric acid MNPs, Core: citric acid: PEG MNPs and Core: citric acid: PEG: ICG: PpIX MNPs showed more than TEM size. In MNPs the smaller the nanoparticle, due to the radius of curvature effect, have significant differences in the size between DLS and TEM. For MNPs in the size range of 20 nm as our study, irregularity in shape and poly disparity are other influencing factors in this difference between the size of DLS and TEM [43].

Coatings such as PEG increase the colloidal stability of MNPs. Therefore, we used PEG coating to increase the stability of MNPs, i.e. improve the PDI factor. In general, the colloidal stability of MNP depends on the polymer and coating charge used. According to the ISO report, PDI values less than 0.5 are desirable for using nanoparticles as a drug delivery agent. In our study, the measured PDI was

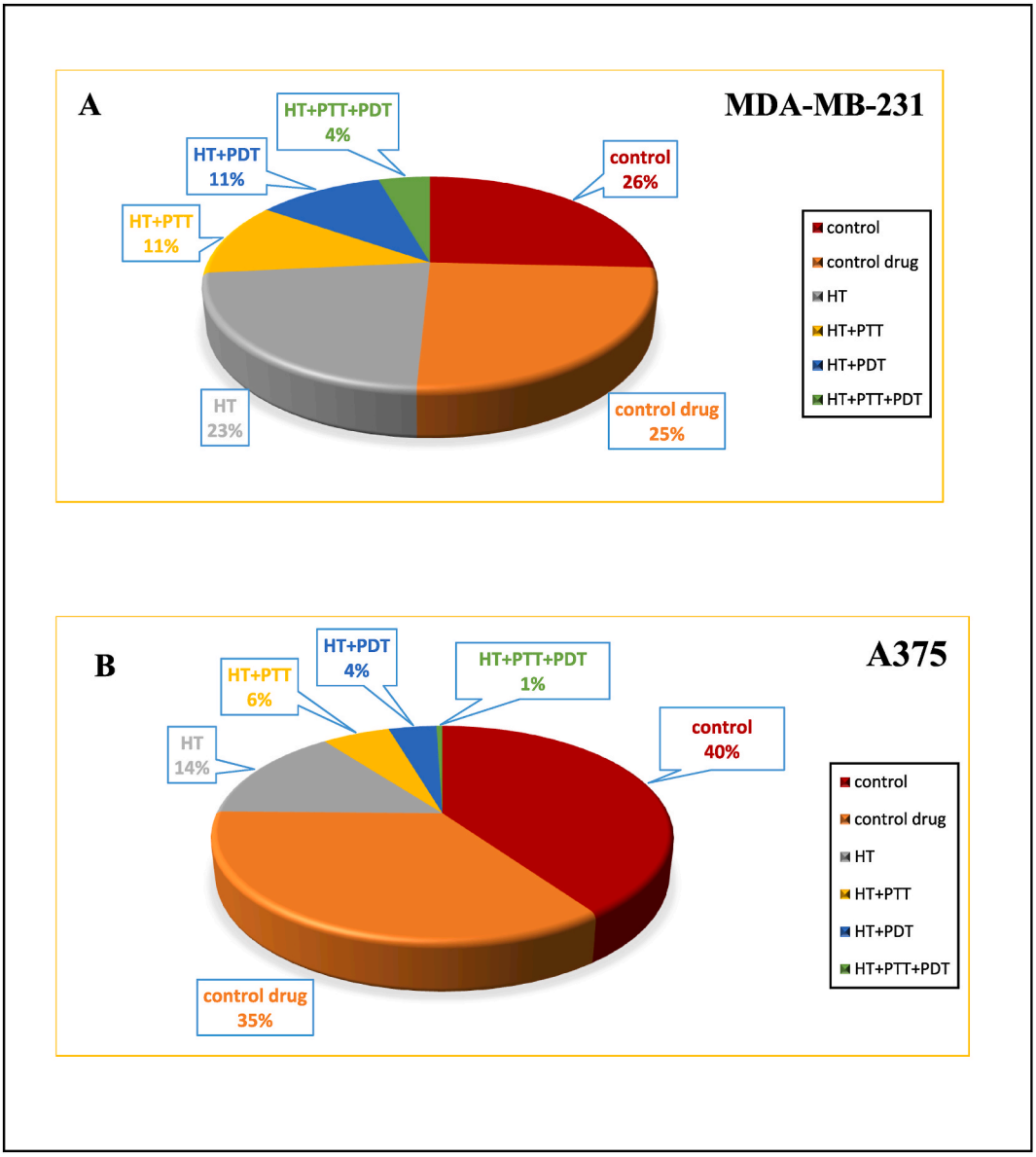

Fig. 13. Flow cytometry pie CHART analyses. A) Percentage of CD133 + $CD44^{+}$ cell in single or multiple treatments of MDA-MB-231 cell line. B) Percentage of CD133 + $CD44^{+}$ cell in single or multiple treatments of A375 cell line.

less than 0.5 in all synthesis steps except for Core: citric acid MNPs. It should be noted that the high PDI can be due to the aggregation and oligomerization of MNs. Zeta potential of MNPs is also one of the indicators of colloidal stability. At low zeta potentials (close to zero), particles are not repelled and colloids accumulate due to surface adsorption forces. While at high zeta potentials, colloidal accumulation is prevented. The nanostructures synthesized in this research with a zeta potential higher than 14 with a negative charge on the surface create a repulsive force between the particles. Therefore, they prevented their accumulation and led to the stability of nanoparticles [44]. So that after the coating of acetic acid and PEG and loading of sensitizers, the zeta potential changed from −14.6 to −22.1, which indicated better nanoparticle stability.

TEM results demonstrated that the Core MNPs has an amorphous and irregular structure. Influences such as pH, concentration of precursor s, reaction temperature, reflux time and the gas environment in which the reaction is performed are among the influencing factors in the size distribution and morphology of nanoparticles that in co-precipitation method. In our study, we used pH of 12.4, reflux time of 3 h, and argon gas flux to reach the desired size of nanoparticle. In our study the important factor that affected the shape and morphology of nanostructures more than other factors were the temperature of the reaction solution. The low temperature (80 °C) during the synthesis led to the creation of Core MNPs with an irregular and amorphous shape. This is consistent with the study of Gomeshis et al. who synthesized magnetite at different temperatures. In this study, the lowest temperature of the synthesis solution

Table 3
Combination Indices (CIs) for different combination of treatment with Core: citric acid: PEG: ICG: PpIX MNPs.

(MDA -MB-231)				A375			
Core: citric acid: PEG: ICG: PpIX MNPs				Core: citric acid: PEG: ICG: PpIX MNPs			
Treatment condition(min)			CIs average ± SD	Treatment condition(min)			CIs average ± SD
MHT=1+PDT=1	MHT=3+PDT=3	MHT=3+PDT=5		MHT=1+PDT=1	MHT=3+PDT=3	MHT=3+PDT=5	
0.89	1.09	2.07	1.35±0.06	1.04	1.21	1.69	1.31±0.06
MHT=1+PTT=1	MHT=3+PTT=3	MHT=3+PTT=5	CIs average ± SD	MHT=1+PTT=1	MHT=3+PTT=3	MHT=3+PTT=5	CIs average ± SD
0.83	0.84	1.77	1.15±0.05	0.99	0.66	1.62	1.09±0.05
MHT=1+PTT=1 +PDT=1	MHT=3+PTT=3 +PDT+3	MHT=3+PTT=5+ PDT=5	CIs average ± SD	MHT=1+PTT= 1+PDT=1	MHT=3+PTT= 3+PDT+3	MHT=3+PTT=5 +PDT=5	CIs average ± SD
0.73	1.1	2.17	1.33±0.06	0.83	0.65	2.54	1.34±0.06

Table 4
Combination Indices (CIs) for different combination of treatment with Core: citric acid MNPs, Core: citric acid: PEG MNPs.

Core: citric acid: PEG MNPs \ Treatment condition(min)	MHT=3+PDT=5	MHT=3+PTT=5	MHT=3+PDT=5+PTT=5
CIs(MDA-MB-231)	1	0.86	0.90
CIs (A375)	0.84	0.80	0.79
Core: citric acid MNPs \ Treatment condition(min)	MHT=3+PDT=5	MHT=3+PTT=5	MHT=3+PDT=5+PTT=5
CIs(MDA-MB-231)	0.82	0.80	0.75
CIs (A375)	0.89	0.85	0.75

was 120° Celsius, amorphous and irregular nanoparticles were synthesized, and more homogeneous nanoparticles were formed at higher temperatures. The chemical composition and size of magnetic nanostructures are very effective in improving the heating efficiency of magnetic hyperthermia [45,46]. Therefore, in our study, we used iron and cobalt for synthesis. And in addition, the final MNP size was ~13 nm, which leads to better thermal efficiency.

The size obtained from the SEM of Core: citric acid: PEG: ICG: PpIX MNPs was in the range of 13 nm using Image j software. According to these image, Core: citric acid: PEG: ICG: PpIX MNPs (Final NP) has an irregular shape. The reason for the larger size displayed in SEM images compared to TEM may be due to aggregation, which is the result of van der Waals forces between particles. MNPs are agglomerated due to high surface energy between nanoparticles and magnetic dipole-dipole interactions.

By examining the XRD pattern of cobalt ferrite, the XRD peak at θ2 at 35.7° indicates the Core MNPs crystal plates with an interlayer distance of 3.83 Å. Therefore, the Core MNPs crystal size by the maximum peak (311) was calculated about 11.67 nm [35]. Our finding was conforming with Humbe et al. study which get nine peak in XRD of their NiCuZnFe2O4 nanoparticles (the same as our peaks in XRD). Their sharp peak was 311 like our study but they get crystal size of 23–34 nm [47]. In this study like Sandeep work, XRD parameters were measured in the angle range of 20–80° for their ZnMgFeGdxO4 nano ferrites. they also find a sharp peak in 311 [48].

According to VSM curve of Core: citric acid MNPs and Core: citric acid: PEG MNPs absence of Mr and Hc confirm that both of them are superparamagnetic [49]. VSM without hysteresis loop is one of properties of superparamagnetic material which can happen for small nanoparticles with increase surface area. Our MNPs with size of ~13 nm obey this law too [50].

Presence of citric acid on the surface of Core MNPs is confirmed in the FTIR spectrum through the peaks in the region of 3500–2800 which are related to the functional groups of citric acid attached to the Core MNPs. In general, to confirm the existence of citric acid on the surface of cobalt ferrite NPs, the FTIR spectrum would show characteristic peaks related to the functional groups present in citric acid. Citric acid contains carboxylic acid groups (-COOH), hydroxyl groups (-OH), and carbonyl groups (C═O). Therefore, in the FTIR spectrum of ferrite-citric acid NPs, we would expect to observe absorption peaks around: The carboxylic acid group: A broad peak between 3393 cm and 1 due to the stretching vibration of –COOH. The hydroxyl group: A broad peak around 3393 cm-1 due to the stretching vibration of –OH. The carbonyl group: A peak around 1612 cm-1 due to the stretching vibration of C═O. The presence of these characteristic peaks in the FTIR spectrum would indicate the existence of citric acid on the surface of cobalt ferrite NPs [51].. The broad peak located at 3418.85 cm^{-1} is related to the stretching vibration of the hydroxyl group of polyethylene glycol, which overlaps with the peak of the OH group on the surface of $CoFe_2O_4$ MNPs. Meanwhile, the existence of a set of peaks at 2872.24 cm^{-1} is related to C–H stretching vibrations of aliphatic polyethylene glycol. So PEG contains repeating units of ethylene oxide (-CH2-CH2-*O*-) and has characteristic peaks at:C–H stretching vibrations: Peaks around 2873 cm-1. C–O stretching vibrations: A peak around 1100-1300 cm-1. C–*O*–C stretching vibrations: Peaks around 1105 cm-1. The presence of these PEG-related peaks in the FTIR spectrum would confirm the existence of PEG on the surface of cobalt ferrite NPs [52]. Citric acid coating was chosen for several reasons. Citric acid provides a good platform for PEG binding, and the PEG itself subsequently causes better loading of ICG and PpIX. This particle is multifunctional and is also considered for intra-body applications in future, so the issue of selective cell absorption was also considered in its design. The citric acid cycle plays important rule in aerobic respiration, and creating energy for in mitochondria. Includes eight chemical reactions in which citrate is one of that products. Both citrate and citric acid inhibit tumor cell propagation and growth [53,54] spatially in breast cancer cells by increasing lipid biosynthesis and causing cell aging [55]. Cancer cells or cancer stem cells have a high metabolism to fulfill augmented energy demands for their, differentiation, proliferation, and progress, in which citrate acting an essential role in it [56]. Metabolism -targeted therapy is new strategy to overcoming cancer [57,58]. Citrate has important role in metabolic regulation [59]. So that extracellular citrate execution can have not only inhibitory effects on cancer cells, but also have synergism effect when it used with other conventional treatments. Using of high-dose citrate rise the intracellular citrate that cause antitumor effects. While low concentration of citric acid cause cell aging which can weakens tumor progress and improves the results of other treatment. Due to the fact that citrate plays an important role in providing intracellular energy [60,61], we propose a theory that having citric acid coating of nanoparticles can cause the selective uptake of the nanoparticles into CS and CSC due to the difference among the metabolic needs of normal cells and cancerous or cancer stem cells and this itself causes the passive targeting of this nanoparticle into the cancer cells [62].

Temperature increase in MHT be influenced by on the shape, size, nanoparticle coating and the composition of the nanoparticle, concentration and external factors such as field strength frequency, the duration of the MF applied and the viscosity of the solvent [63]. Considering the stability of external factors, our synthesized MNPs with a size of ~13 nm and a shape of cubic, in concentrations between 0.02 and 0.16 causes an increase in temperature with increasing concentration. This increase in temperature is significant in Core: citric acid: PEG: ICG: PpIX MNPs compare to Core: citric acid: PEG MNPs and it is more than Core: citric acid MNPs. Because there are many interfering factors and exceptions in magnetic hyperthermia, this may not be true for nanoparticles with other sizes and other concentration. MNPs in a larger size, under a threshold size (for magnetic iron oxide NP is about 128 nm), become single-domain, and called superparamagnetic (like our study NPs size range), unlike large nanoparticles, which have hysteresis loss, this superparamagnetic NPs have Néel and Brownian relaxation for loss electromagnetic energy and converted to heat like our MNPs [64]. So in very high concentrations, because the phenomenon of aggregation has occurred and the distance between particles decreases and Because dipole-dipole interaction is more depend on the Néel relaxation time and Brownian relaxation is much less sensitive to the concentration, the increasing concentration from a certain limit, increases Néel relaxation and SAR and as a result of the decreased temperature. For this reason, in order to have noticeable temperature raise, optimum concentration should be founded. So any factor causes aggregation can have inverse affect in SAR. Our Core: citric acid: PEG: ICG: PpIX MNPs has good combination of PDI and zeta potential and the result of those curves feet our expectation. Alexander et al. FluidmagDX iron oxide nanoparticle with TEM size of ~84 nm, magnetic field strength of 10 mT, frequency of 140 kHz, time of ~45 min and concentration of 5 mg/ml demonstrated ΔT~9C° [65], While in our study with Core: citric acid: PEG: ICG: PpIX MNPs with size~ 13 nm, magnetic field strength of 33.5 mT, frequency of 425 kHz, time of 6 min and concentration of 0.16 mg/ml we achieved ΔT~15C°. This study was in agreement with our study. In both of them increase in temperature was dependent on the concentration. Beside that our Core: citric acid: PEG: ICG: PpIX MNPs has cubic shape, which enormous studies show better efficiency of cubic NPs in comparison to spherical NPs (Core: citric acid MNPs, and Core: citric acid: PEG MNPs). Our finding is in agreement with Song et al. study who compare heat efficacy on quasi-cubical and spherical Fe3O4nanoparticles [66]. Like concentration, for viscosity of solvent there is the optimal domain in with before and after that heating behavior of magnetic nanoparticle change. Brownie relaxation was more affected by viscosity than Néel relaxation. At high viscosities, it is eliminated and the SAR decreases [67]. In order to keep the viscosity variable constant, we carried out all the aquatic environment studies in water. Song et al. showed that In contrast, at very low particle concentrations (like our paper) the

particles stand far from each other and inter-particle dipolar interaction declines radically [68]. Also conductivity of coating and its thickness is another important factor affects SAR and heat production. Gonzalez et al. covered magnetic iron oxide nanoparticle (MIONs) with SiO2 which has little heat conduction result in reduction of heating efficiency [69]. Liu et al. evaluated the effect of nanoparticle thickness on heating efficiency. They used polyethylene glycol (PEG) with different thickness (2000 to 20,000 Da). They conducted that thinner layer has good heat conductivity and dispensability in comparison to thick shell that because of the increased Brownian loss [70]. We also used thin layer of PEG in our study in order to increase dispensability and biocompatibility of MNPs. So MNPs with PEG layer has better heat efficiency according to Fig. 2. By looking at result of conductivity, it can conclude that reduction in conductivity in Core MNPs after covering by citric acid and PEG showed that these coatings have been successfully drawn on Core MNPs s and this reduction cause lower heat transition (Fig. 2). Beside the ability of increasing temperature, ROS production of Core: citric acid: PEG: ICG: PpIX MNPs were evaluated. According to studies MNPs can act as peroxidase and be able to produce hydroxyl radicals (°OH) by catalyzing Hydrogen peroxide (H2O2) [71]. Ziya et al. showed that even in absence of magnetic hyperthermia MNP can produce amount of ROS (especially °OH). They use N,N-dimethyl-*p*-phenylenediamine (DMPD) probe (°OH detector) and F3O4 NPs with the size of 20–30 nm. They showed that in concentration around 0.1 mg/ml, absorbance of solution (F3O4 NP + DMPD) was around 0.6 [72]. While we sense among of °OH with Terephthalic acid + Core: citric acid: PEG: ICG: PpIX MNPs in presence of magnetic field and achieve high amount of °OH production in with combination of MNPs and magnetic field. Fig. 8 shows that Core: citric acid: PEG: ICG: PpIX MNPs -induced production of °OH in magnetic field has a direct relationship with the time of application of the magnetic field. Terephthalic acid alone is non-fluorescent and becomes fluorescent when combined with hydroxyl radical (°OH). So, high level of °OH in solution, indicates the high level of fluorescence caused by this compound [73].

Toxicity of MNPs is depend on concentration of MNPs. Mohammadi et al. evaluate toxicity of CoFe2O4MNPs) size∼10 nm) they find no toxicity up to concentration of 0.04 mg/ml in 24h for MAD-MB-231. In our study with the same cell line and core but with different coating we found viability of 96%,89% and 82% for Core: citric acid MNPs, Core: citric acid: PEG MNPs and Core: citric acid: PEG: ICG: PpIX MNPs, respectively [33]. Therefore, it can be concluded that citric and PEG coatings cause more penetration of nanoparticles into the cell and increase its toxicity and by looking at cell viability this effect with PEG coating is more than acid. It was agreed in both cell line in our study Abudayyak et al. estimate the toxicity of Core MNPs (size∼39) in NRK-52E kidney they found that in concentration up to 0.1 mg/ml viability was between ∼ 85 and 100 [74]. It is somehow agreed with our study Momin et al. worked on toxicity of Core MNPs (size 8–10 nm) on human lymphocytes and found that in concentration of 0.1 mg/ml cell viability was ∼75% [75], while we achieved this viability in lower concentration. Core MNPs toxicity still argued and mostly it depends on kind of cell line.

According to Fig. 2 in both cell lines cell survival depends on time of applying magnetic field in constant concentration, magnetic file strength and frequency. It is agreed with study of Kekalo et al. they showed that increase in temperature depends on the strength of the magnetic field and the time of MF application, and in a constant magnetic field, the temperature rises with time [76]. Fig. 4 can be explained according to Fig. 5. We observed $\Delta T = 19.6\ ^{\circ}C$ between 0 and 3 min of irradiation and $\Delta T = 35.2\ ^{\circ}C$ between 0 and 6 min in Fig. 11. It means that 3 min irradiation here is threshold pint for hyperthermia-induced effect. Up to 3 min temperature reached maximum ∼41.6 and for 6 min irradiation temperature achieved ∼57.2 taking into account that the initial temperature was 22 °C. At temperatures lower than 46 °C, the functions of intracellular proteins are disrupted and cause apoptosis [77], but temperatures above 46° cause direct cell death through thermal ablation consist of necrosis, coagulation or carbonization [78]. So in survival cure of MHT cell survival dramatically drop to 15.55% and 17.21% in MAD-MB-231 and A375, respectively.

In all combination therapy include MHT + PDT, MHT + PTT, and MHT + PTT + PDT we observed a decrease in survival depending on the duration of light radiation and magnetic field. In both cell lines cell survival in Core: citric acid: PEG: ICG: PpIX MNPs were lower than Core: citric acid MNPs and Core: citric acid: PEG MNPs. High thermal efficiency of the PEG coating in the MF due to the better stability of the nanoparticle compared to the citric causes a better temperature increase and more cell death. Good zeta potential and conductivity of Core: citric acid: PEG: ICG: PpIX MNPs in compare to Core: citric acid: PEG MNPs and Core: citric acid MNPs prevent aggregation and making large NP and prepare best heat transform, so it causes the best efficiency (decrease cell viability) in all treatment groups in both cell lines (P-value$<$0.001). In the presence of Core: citric acid: PEG: ICG: PpIX MNPs in MDA-MB-231 cell line there is synergism effect in MHT = 3 + PDT = 3 and MHT = 3 + PDT = 5, while there is synergism effect in all combination groups of MTH + PDT in A375 cell line. Combinational treatment groups of MTH + PTT in A375 and MDA-MB -231 cell lines just MHT = 3 + PTT = 5 has synergism effect. The percentage of photothermal agent loading was lower than photodynamic so efficiency of photothermal treatments seems to be lower than that of photodynamic. Unlike A375 cell line which showed synergism in only in MHT = 3 + PTT = 5 + PTT = 5, MDA-MB -231 cell line also demonstrated synergism in MHT = 3 + PTT = 3 + PTT = 5. In contrast Core: citric acid MNPs and Core: citric acid: PEG MNPs proved no synergism effect in any combination groups, just for MDA-MB -231 cell line additive effect in MTT = 3 + PDT = 5 was seen. Therefore, efficiency of Core: citric acid: PEG: ICG: PpIX MNPs has been better than other MNPs in combined treatments. These cell survival results obtained from MTT assay and were well agreed with flow cytometry outcome. shows some study used single or combination therapy on cancer cell or tissue and were confirm the benefits of multiple treatment in comparison to single treatment. In general, according to the studies, the combination of methods such as MHT with PTT and PDT improves the disadvantages of each of the individual therapies. For example, magnetic hyperthermia removes the limitation of penetration depth related to photothermal treatment and the use of these two results in better temperature increase. The simultaneous use of photodynamic with MHT also multiplies the effect of these combined treatments due to the PDT-Induced radical toxicity by weaken theheat-shock cellular defense [79,80]. In addition, the dose of the nanoparticle, frequency and magnetic field, light exposure dose used in the combined treatments are much less than individual treatments, and itself helps to maintain healthy tissue in next in vivo studies [81]. Also these combination therapies showed good effect on reduction of CD44 + $CD24^{-}$and CD133 + $CD44^{+}$ cells which are well-known surface biomarkers of CSCs [82]. This reduction in CD44 + $CD24^{-}$in A375 cell line was more significant between single treatment and combined treatments (P-value$<$0.001), but there was no substantial difference between MHT + PDT and

MHT + PTT (P-value>0.05), while for all groups of treatment in MDA-MB -231 cell line there was noticeable variance. According to Fig. 13 these combined treatment act well for eradication of CD133 + $CD44^{+}$ in A375 cell line than MDA-MB -231 cell line. Some studies demonstrate effect of MHT on CSCs as shown in Table 1S. Table 2S shows some studies using MHT and MNPs on CSCs or NCSs. Several studies have been done in the field of photodynamic and photothermal alone or together with chemotherapy and radiotherapy on cancer stem cells, but in relation to combined photodynamic and photothermal treatments with magnetic hyperthermia, no study has been done on cancer stem cells. In our study, for the first time, we investigated the effect of combined treatments of magnetic hyperthermia with photodynamic, magnetic hyperthermia with photothermal and combination treatment of magnetic hyperthermia/photothermal/photodynamic therapy on eradication of cancer stem cells. Table 1S shows some studies using single or multiple treatments on cell or tissue and Table 2S demonstrates some research information using MHT and MNPs on CSCs or NCSs.

5. Conclusion

We successfully synthesis a novel multi-functional magnetic nanoparticle which is capable to be used simultaneously in photodynamic and photothermal hyperthermia treatments. ICG and PpIX are photosensitizers that are used in photothermal, respectively that play the role of light-based treatment of this nanoparticle and ferrite cobalt is magnetic core of this nanoparticle which is responsible for the magnetic hyperthermia. The navel synthesized Core: citric acid: PEG: ICG: PpIX MNPs has a high efficiency in creating heat and producing hydroxyl radicals in magnetic hyperthermia. In addition, the obtained results showed that when magnetic hyperthermia is used together with light-based treatments, due to the synergistic created effect that, the effect of combination treatment is greater than that of single treatments. Therefore, it is highly effective in reducing the population of CSCs compared to single treatments in both cell lines Then, because of the resistance of stem cells to common cancer treatments such as drug-based and radiation-based treatments, and the favorable results obtained from the combinational effects of photodynamic, photothermal and magnetic hyperthermia treatments on CSCs, more attention should be given to non-ionizing methods in this regard. Studies such as gene expression and signaling pathways regarding the use of these treatments should also be done in order to understand the benefits of this issue and to find a suitable method to solve the problem of tumor recurrence.

Author contribution statement

Bahareh Khalili Najafabad: Performed the experiments; Analyzed and interpreted the data; Wrote the paper.

Neda Attaran: Mehdi Barati: Zahra Mahmoudi: Analyzed and interpreted the data. Mahmoud Mahmoudi: Conceived and designed the experiments. Ameneh Sazgarnia: Conceived and designed the experiments; Analyzed and interpreted the data; Contributed reagents, materials, analysis tools or data.

Data availability statement

Data included in article/supp. material/referenced in article.

Declaration of competing interest

The authors declare that they have no known competing financial interests or personal relationships that could have appeared to influence the work reported in this paper.

Appendix A. Supplementary data

Supplementary data to this article can be found online at https://doi.org/10.1016/j.heliyon.2023.e19893.

References

[1] M. Faraji, Y. Yamini, M. Rezaee, Magnetic nanoparticles: synthesis, stabilization, functionalization, characterization, and applications, J. Iran. Chem. Soc. 7 (1) (2010) 1–37.
[2] B. Somvanshi, S, et al., Multifunctional nano-magnetic particles assisted viral RNA-extraction protocol for potential detection of COVID-19, Mater. Res. Innovat. 25 (3) (2021) 169–174.
[3] L. Garcell, et al., Interfacial and rheological characteristics of maghemite aqueous suspensions, J. Colloid Interface Sci. 205 (2) (1998) 470–475.
[4] C.R. Kalaiselvan, et al., Manganese ferrite (MnFe2O4) nanostructures for cancer theranostics, Coord. Chem. Rev. 473 (2022), 214809.
[5] V. Cabuil, Dekker Encyclopedia of Nanoscience and Nanotechnology, Chapter 119 Magnetic Nanoparticles: Preparation and Properties, Roldan group puplications, 2004.
[6] P.B. Kharat, et al., Induction heating analysis of surface-functionalized nanoscale CoFe2O4 for magnetic fluid hyperthermia toward noninvasive cancer treatment, ACS Omega 5 (36) (2020) 23378–23384.
[7] C. Thakral, J. Alhariri, J.L. Abraham, Long-term retention of gadolinium in tissues from nephrogenic systemic fibrosis patient after multiple gadolinium-enhanced MRI scans: case report and implications, Contrast Media Mol. Imaging 2 (4) (2007) 199–205.
[8] L.L. Muldoon, et al., Imaging, distribution, and toxicity of superparamagnetic iron oxide magnetic resonance nanoparticles in the rat brain and intracerebral tumor, Neurosurgery 57 (4) (2005) 785–796.
[9] H.S. Choi, et al., Renal clearance of quantum dots, Nat. Biotechnol. 25 (10) (2007) 1165–1170.

[10] P. Ayyub, et al., Size-induced structural phase transitions and hyperfine properties of microcrystalline Fe2O3, J. Phys. C Solid State Phys. 21 (11) (1988) 2229.
[11] H. Grossman, et al., Detection of bacteria in suspension by using a superconducting quantum interference device, Proc. Natl. Acad. Sci. USA 101 (1) (2004) 129–134.
[12] C. Dai, et al., Photonic/magnetic hyperthermia-synergistic nanocatalytic cancer therapy enabled by zero-valence iron nanocatalysts, Biomaterials 219 (2019), 119374.
[13] S.B. Somvanshi, P.B. Kharat, K. Jadhav, Surface functionalized superparamagnetic Zn-Mg ferrite nanoparticles for magnetic hyperthermia application towards noninvasive cancer treatment, in: Macromolecular Symposia, Wiley Online Library, 2021.
[14] S.B. Somvanshi, et al., Core-shell structured superparamagnetic Zn-Mg ferrite nanoparticles for magnetic hyperthermia applications, J. Alloys Compd. 947 (2023), 169574.
[15] P.B. Kharat, et al., Synthesis, characterization and hyperthermic evaluation of PEGylated superparamagnetic MnFe2O4 ferrite nanoparticles for cancer therapeutics applications, in: Macromolecular Symposia, Wiley Online Library, 2021.
[16] A. Nikitin, et al., Synthesis of iron oxide nanorods for enhanced magnetic hyperthermia, J. Magn. Magn Mater. 469 (2019) 443–449.
[17] M. Huo, et al., Tumor-selective catalytic nanomedicine by nanocatalyst delivery, Nat. Commun. 8 (1) (2017) 1–12.
[18] R.D. Issels, et al., Neo-adjuvant chemotherapy alone or with regional hyperthermia for localised high-risk soft-tissue sarcoma: a randomised phase 3 multicentre study, Lancet Oncol. 11 (6) (2010) 561–570.
[19] T. Reya, et al., Stem cells, cancer, and cancer stem cells, Nature 414 (6859) (2001) 105–111.
[20] M.R. Atashzar, et al., Cancer stem cells: a review from origin to therapeutic implications, J. Cell. Physiol. 235 (2) (2020) 790–803.
[21] A. Jaggupilli, E. Elkord, Significance of CD44 and CD24 as cancer stem cell markers: an enduring ambiguity, Clin. Dev. Immunol. (2012), 2012.
[22] I.L. Botchkina, et al., Phenotypic subpopulations of metastatic colon cancer stem cells: genomic analysis, CANCER GENOMICS PROTEOMICS 6 (1) (2009) 19–29.
[23] M.T. Wan, J.Y. Lin, Current evidence and applications of photodynamic therapy in dermatology, Clin. Cosmet. Invest. Dermatol. 7 (2014) 145.
[24] L. Cheng, et al., Functional nanomaterials for phototherapies of cancer, Chem. Rev. 114 (21) (2014) 10869–10939.
[25] L. Zou, et al., Current approaches of photothermal therapy in treating cancer metastasis with nanotherapeutics, Theranostics 6 (6) (2016) 762.
[26] G.L. Baiocchi, M. Diana, L. Boni, Indocyanine green-based fluorescence imaging in visceral and hepatobiliary and pancreatic surgery: state of the art and future directions, World J. Gastroenterol. 24 (27) (2018) 2921.
[27] S.M. Sharker, et al., pH triggered in vivo photothermal therapy and fluorescence nanoplatform of cancer based on responsive polymer-indocyanine green integrated reduced graphene oxide, Biomaterials 61 (2015) 229–238.
[28] Y. Liu, et al., Tumor-triggered drug release from calcium carbonate-encapsulated gold nanostars for near-infrared photodynamic/photothermal combination antitumor therapy, Theranostics 7 (6) (2017) 1650.
[29] G. Sheng, et al., Encapsulation of indocyanine green into cell membrane capsules for photothermal cancer therapy, Acta Biomater. 43 (2016) 251–261.
[30] A.D. Garg, et al., ROS-induced autophagy in cancer cells assists in evasion from determinants of immunogenic cell death, Autophagy 9 (9) (2013) 1292–1307.
[31] R. Philip, et al., Absorption and fluorescence spectroscopic investigation of indocyanine green, J. Photochem. Photobiol. Chem. 96 (1–3) (1996) 137–148.
[32] S.R. Patade, et al., Self-heating evaluation of superparamagnetic MnFe2O4 nanoparticles for magnetic fluid hyperthermia application towards cancer treatment, Ceram. Int. 46 (16) (2020) 25576–25583.
[33] B.K. Najafabad, et al., Effect of photothermal and photodynamic therapy with cobalt ferrite superparamagnetic nanoparticles loaded with LCG and PpIX on cancer stem cells in MDA-MB-231 and A375 cell lines, Photodiagnosis Photodyn. Ther. (2023), 103648.
[34] A.K. Croker, et al., High aldehyde dehydrogenase and expression of cancer stem cell markers selects for breast cancer cells with enhanced malignant and metastatic ability, J. Cell Mol. Med. 13 (8b) (2009) 2236–2252.
[35] Z. Mohammadi, et al., Superparamagnetic cobalt ferrite nanoparticles as T 2 contrast agent in MRI: in vitro study, IET Nanobiotechnol. 14 (5) (2020) 396–404.
[36] Z.E. Gahrouei, S. Labbaf, A. Kermanpur, Cobalt doped magnetite nanoparticles: synthesis, characterization, optimization and suitability evaluations for magnetic hyperthermia applications, Phys. E Low-dimens. Syst. Nanostruct. 116 (2020), 113759.
[37] F. Daneshvar, et al., Combined X-ray radiotherapy and laser photothermal therapy of melanoma cancer cells using dual-sensitization of platinum nanoparticles, J. Photochem. Photobiol. B Biol. 203 (2020), 111737.
[38] H.K. Can, et al., Preparation, characterization and dynamical mechanical properties of dextran-coated iron oxide nanoparticles (DIONPs), Artif. Cell Nanomed. Biotechnol. 46 (2) (2018) 421–431.
[39] K. Takahashi, et al., Precise measurement of the size of nanoparticles by dynamic light scattering with uncertainty analysis, Part. Part. Syst. Char. 25 (1) (2008) 31–38.
[40] J. Lim, et al., Characterization of magnetic nanoparticle by dynamic light scattering, Nanoscale Res. Lett. 8 (2013) 1–14.
[41] L. Zhang, R. He, H.-C. Gu, Oleic acid coating on the monodisperse magnetite nanoparticles, Appl. Surf. Sci. 253 (5) (2006) 2611–2617.
[42] Z. Wang, et al., Reconstructing a solid-solid phase transformation pathway in CdSe nanosheets with associated soft ligands, Proc. Natl. Acad. Sci. USA 107 (40) (2010) 17119–17124.
[43] M. Gittings, D. Saville, The determination of hydrodynamic size and zeta potential from electrophoretic mobility and light scattering measurements, Colloids Surf. A Physicochem. Eng. Asp. 141 (1) (1998) 111–117.
[44] M.S. Darwish, et al., Functionalized magnetic nanoparticles and their effect on Escherichia coli and Staphylococcus aureus, J. Nanomater. 16 (1) (2015) 89, 89.
[45] F. Liu, et al., Size-controlled synthesis of CoFe2O4 nanoparticles potential contrast agent for MRI and investigation on their size-dependent magnetic properties, J. Nanomater. 2013 (2013) 127, 127.
[46] N. Torres-Gómez, et al., Shape tuning of magnetite nanoparticles obtained by hydrothermal synthesis: effect of temperature, J. Nanomater. 2019 (2019).
[47] A.V. Humbe, et al., Cation distribution, magnetic and hyperfine interaction studies of Ni–Zn spinel ferrites: role of Jahn Teller ion (Cu 2+) substitution, Materials Advances 1 (4) (2020) 880–890.
[48] S.B. Somvanshi, et al., Structural, thermal, spectral, optical and surface analysis of rare earth metal ion (Gd3+) doped mixed Zn–Mg nano-spinel ferrites, Ceram. Int. 46 (9) (2020) 13170–13179.
[49] A. Alsmadi, et al., Magnetic study of M-type doped barium hexaferrite nanocrystalline particles, J. Appl. Phys. 114 (24) (2013), 243910.
[50] T. Theivasanthi, M. Alagar, Innovation of superparamagnetism in lead nanoparticles, arXiv preprint arXiv:1402.1431 (2014).
[51] H. Ahankar, et al., Magnetic cobalt ferrite nanoparticles functionalized with citric acid as a green nanocatalyst for one-pot three-component sonochemical synthesis of substituted 3-pyrrolin-2-ones, Res. Chem. Intermed. 45 (10) (2019) 5007–5025.
[52] N. Hendi, et al., Study of the parameters affecting the loading of fluorescein on coated gold nanoparticles: promising nanostructure for cancer diagnosis, Anti Cancer Agents Med. Chem. 21 (17) (2021) 2429–2442.
[53] J.-G. Ren, et al., Citrate suppresses tumor growth in multiple models through inhibition of glycolysis, the tricarboxylic acid cycle and the IGF-1R pathway, Sci. Rep. 7 (1) (2017) 1–13.
[54] M. Ayat, Citric acid inhibits clonogenic power and anchorage-independent growth of glioma cells, The Egyptian Journal of Hospital Medicine 77 (1) (2019) 4824–4831.
[55] Y. Zhao, et al., Citrate promotes excessive lipid biosynthesis and senescence in tumor cells for tumor therapy, Adv. Sci. 9 (1) (2022), 2101553.
[56] L.C. Costello, R.B. Franklin, A review of the important central role of altered citrate metabolism during the process of stem cell differentiation, J. Regen. Med. Tissue Eng. 2 (2013).
[57] S. Beloribi-Djefaflia, S. Vasseur, F. Guillaumond, Lipid metabolic reprogramming in cancer cells, Oncogenesis 5 (1) (2016) e189, e189.
[58] K. Vasan, M. Werner, N.S. Chandel, Mitochondrial metabolism as a target for cancer therapy, Cell Metabol. 32 (3) (2020) 341–352.
[59] P. Icard, et al., Understanding the central role of citrate in the metabolism of cancer cells and tumors: an update, Int. J. Mol. Sci. 22 (12) (2021) 6587.
[60] K. Jordan, et al., Potential involvement of extracellular citrate in brain tumor progression, Curr. Mol. Med. 22 (6) (2022) 506–513.
[61] L. Huang, et al., Targeting citrate as a novel therapeutic strategy in cancer treatment, Biochim. Biophys. Acta Rev. Canc 1873 (1) (2020), 188332.

[62] C. von Schirnding, et al., Synergistic combination of calcium and citrate in mesoporous nanoparticles targets pleural tumors, Chem 7 (2) (2021) 480–494.
[63] D. Chang, et al., Biologically targeted magnetic hyperthermia: potential and limitations, Front. Pharmacol. 9 (2018) 831.
[64] M. Suto, et al., Heat dissipation mechanism of magnetite nanoparticles in magnetic fluid hyperthermia, J. Magn. Magn Mater. 321 (10) (2009) 1493–1496.
[65] A.S. Eggeman, et al., Size and concentration effects on high frequency hysteresis of iron oxide nanoparticles, IEEE Trans. Magn. 43 (6) (2007) 2451–2453.
[66] M. Song, et al., Influence of morphology and surface exchange reaction on magnetic properties of monodisperse magnetite nanoparticles, Colloids Surf. A Physicochem. Eng. Asp. 408 (2012) 114–121.
[67] R.E. Rosensweig, Heating magnetic fluid with alternating magnetic field, J. Magn. Magn Mater. 252 (2002) 370–374.
[68] J. Zhang, C. Boyd, W. Luo, Two mechanisms and a scaling relation for dynamics in ferrofluids, Phys. Rev. Lett. 77 (2) (1996) 390.
[69] M. Gonzalez-Fernandez, et al., Magnetic nanoparticles for power absorption: optimizing size, shape and magnetic properties, J. Solid State Chem. 182 (10) (2009) 2779–2784.
[70] X.L. Liu, et al., Optimization of surface coating on Fe 3 O 4 nanoparticles for high performance magnetic hyperthermia agents, J. Mater. Chem. 22 (17) (2012) 8235–8244.
[71] L. Gao, et al., Intrinsic peroxidase-like activity of ferromagnetic nanoparticles, Nat. Nanotechnol. 2 (9) (2007) 577–583.
[72] Z. Can, et al., Magnetite nanoparticles-based hydroxyl radical scavenging activity assay ofantioxidants using N, N-dimethyl-p-phenylenediamine probe, Turk. J. Chem. 44 (5) (2020) 1366–1375.
[73] X. Wu, et al., Cold-catalytic antitumor immunity with pyroelectric black phosphorus nanosheets, Chem. Sci. 13 (23) (2022) 6842–6851.
[74] M. Abudayyak, T.A. Gürkaynak, G. Özhan, In vitro evaluation of the toxicity of cobalt ferrite nanoparticles in kidney cell, Turkish Journal of Pharmaceutical Sciences 14 (2) (2017) 169.
[75] N. Momin, A. Deshmukh, S. Radha, Synthesis and characterization of CoFe2O4 & NiFe2O4 magnetic nanoparticles for various biomedical applications: cell viability and cell death evaluations, in: Journal of Nano Research, Trans Tech Publ, 2015.
[76] K. Kekalo, et al., Magnetic nanoparticles with high specific absorption rate at low alternating magnetic field, Nano Life 5 (2) (2015), 1550002.
[77] K.S. Sellins, J.J. Cohen, Hyperthermia induces apoptosis in thymocytes, Radiat. Res. 126 (1) (1991) 88–95.
[78] C.S. Kumar, F. Mohammad, Magnetic nanomaterials for hyperthermia-based therapy and controlled drug delivery, Adv. Drug Deliv. Rev. 63 (9) (2011) 789–808.
[79] C. Angelé-Martínez, et al., Reactive oxygen species generation by copper (II) oxide nanoparticles determined by DNA damage assays and EPR spectroscopy, Nanotoxicology 11 (2) (2017) 278–288.
[80] J. Frank, et al., Intensified oxidative and nitrosative stress following combined ALA-based photodynamic therapy and local hyperthermia in rat tumors, Int. J. Cancer 107 (6) (2003) 941–948.
[81] K. Wu, et al., Urchin-like magnetic microspheres for cancer therapy through synergistic effect of mechanical force, photothermal and photodynamic effects, J. Nanobiotechnol. 20 (1) (2022) 1–22.
[82] L. Walcher, et al., Cancer stem cells—origins and biomarkers: perspectives for targeted personalized therapies, Front. Immunol. 11 (2020) 1280.